Bisaldehyde Allosteric Effectors as Molecular Ratchets and Probes†

Telih Boyiri,‡ Martin K. Safo,‡ Richmond E. Danso-Danquah,‡ Jean Kister,§ Claude Poyart,§ and Donald J. Abraham*,‡

Department of Medicinal Chemistry, School of Pharmacy, Medical College of Virginia, Virginia Commonwealth University, Richmond, Virginia 23298-0540, and Physiologie et Physiopathologie Moléculaires du Globule Rouge, INSERM U299, 78, Rue du General Leclerc, 94275 Le Kremlin Bicêtre, France

Received February 24, 1995; Revised Manuscript Received June 27, 1995⊗

ABSTRACT: Four new series of monoaldehyde bisacids and bisaldehyde bisacids with varying chain lengths have been synthesized and evaluated as allosteric effectors of hemoglobin. Molecular modeling, oxygen equilibrium, and crystallographic studies were combined for structure/function studies. Crystallographic analyses of the bisaldehydes reveal that Schiff base interaction occurred exclusively between Val 1α and Lys 99α of the opposite α chain even though the two terminal Val 1α nitrogens are ideally spaced to also form cross-links. The reason for the observed mode of binding appears to be the influence of chain direction set by key substitutions on the bisaldehyde molecule. Even longer chain derivatives that could overcome the direction set by the key functional groups bind in the same manner. These studies support the general conclusion that long flexible molecules prefer to bind along cavity walls, like double-sided molecular sticky tape, rather than span large open spaces with few chances for interaction. The cross-linked bisaldehydes bind at the same site when incubated under both allosteric states and exhibit reduced cooperativity with a significant decrease in oxygen affinity. The chain length acts as a molecular ratchet and dictates the degree of allosteric effect observed. The tighter the cross-link, the greater the constraint on the tense- (T-) state and the stronger the allosteric effect that is produced. The monoaldehyde bisacids bind in the same fashion with Schiff base formation at Val 1α while the acid that replaces the second aldehyde moiety forms a salt bridge with Lys 99α of the opposite subunit. This class of molecules has weaker allosteric effector activity as would be expected with replacement of one covalent bond by a salt bridge. The importance of Lys 99α on the allosteric equilibrium is confirmed.

Hemoglobin (Hb)[1] is a tetrameric allosteric protein that consists of two α and two β subunits arranged around a central water cavity that is bisected by a molecular 2-fold axis. The ability for Hb to release or take up oxygen can be regulated by allosteric effectors; effectors that increase oxygen affinity shift the allosteric equilibrium toward oxy-Hb (R-state), while those that decrease oxygen affinity shift the allosteric equilibrium toward deoxy-Hb (T-state). The central water cavity binds a number of Hb allosteric effectors at both ends and in the middle (Arnone, 1972; Manning & Manning, 1988; Lalezari et al., 1988; Wireko et al., 1991; Wireko & Abraham, 1991).

In an accompanying study (Abraham et al., 1995b) we discovered that structurally similar monoaldehydes that bind to the same protein residue (Val 1α) produce opposite allosteric effects. A hypothesis was proposed to explain the observed diversity in allosteric action. Allosteric effectors that form intersubunit interactions across the symmetry axis in the T-state add further constraint to that state and produce a low-affinity Hb. Effectors that left shift the oxygen equilibrium curve to produce a high-affinity Hb (1) bind with no intersubunit T-state interactions, (2) inhibit nonspecific chloride binding (Perutz et al., 1993), and (3) disrupt the T-state salt or proposed water-mediated bridge between the opposing termini of the α chains (Fermi, 1975).

To further test this hypothesis, we designed and synthesized four new classes of mono- and bisaldehyde allosteric effectors that were carefully constructed to probe hemoglobin structure and function and hopefully provide answers to the following questions:

(1) Can the same aldehyde allosteric effector bind to the same protein residue in both allosteric states?

(2) What structural features of the aldehyde effectors can be modified to increase the constraint in the T-state and produce a desired degree of shift in the allosteric equilibrium?

(3) What key structural components on the aldehyde effectors are necessary to orient their reactive chains to cross-link or interact with desired protein residues?

(4) What structural features of the aldehyde effectors are responsible for the observed direction in shift of the allosteric equilibrium?

† This work was supported in part by NIH HLBI Grant RO-1-32793 (to D.J.A.), Virginia Commonwealth University, and Institut National de la Santé et de la Recherche Médicale, la Fondation pour la Recherehe Médicale, la Faculté de Médecine Paris-Sud et la Direction des Recherches, Etudes et Tecniques.

* Address correspondence to this author.

‡ Virginia Commonwealth University.

§ INSERM.

⊗ Abstract published in *Advance ACS Abstracts,* August 15, 1995.

[1] Abbreviations: Hb, tetrameric human adult hemoglobin; DPG, 2,3-diphosphoglyceric acid; HPLC, high-pressure liquid chromatography; 5-FSA, 5-formylsalicylic acid; HMAB, methyl 2-hydroxy-5-acetalbenzoate; HMB, methyl 4-hydroxybenzoate; MFSA, methyl 5-formyl-2-hydroxybenzoate; 2-BF, 2-(benzyloxy)-5-formylbenzoic acid; 2-PEF, α-(2-carboxy-4-formylphenoxy)-*p*-toluic acid; 12C79, 5-(2-formyl-3-hydroxyphenoxy)pentanoic acid (formerly known as BW12C); ΔP_{50}, the shift in mmHg (relative to control) at the point on the oxygen equilibrium curve where 50% of Hb is saturated with oxygen; PTH, phenylthiohydantoin; K_T, oxygen binding constant to the deoxy (T) state; K_R, oxygen binding constant to the oxy (R) state; $L = T_o/R_o$, the allosteric equilibrium constant; % T_3, percentage of triligated oxygen in the T-state; i_s (−log L/c), switchover point of the allosteric equilibrium in terms of the number of oxygens bound to Hb.

0006-2960/95/0434-15021$09.00/0

MATERIALS AND METHODS

Materials and General Procedure. All reagents and starting materials for the synthesis were purchased from Aldrich Chemical Co., Lancaster, Kodak, and Fluka and were used directly without further purification. Solvents were purchased from Fisher Scientific Co. and Aldrich Chemical Co. Methanol and acetone were purchased as HPLC grade and used without purification. THF was dried over lithium aluminum hydride and then distilled.

Silica gel coated plates (0.25 mm thickness) were purchased from Analtech Inc. and used for thin-layer chromatography (TLC). The separations were spotted by visualizing under UV light (254 μL), iodine chamber, or Dragendorff's reagent. Flash chromatographic separations were done using Merck, grade 9385, 230−400 mesh, 60 Å silica gel. Modeling was performed using SYBYL, Molecular Modeling Software, version 6.1, TRIPOS, Inc., St. Louis, MO.

The proton magnetic resonance (^{1}H NMR) spectra were recorded on a GE 300 MHz spectrometer and are reported in parts per million (δ ppm) using tetramethylsilane (TMS) as an internal standard. Elemental analyses were obtained from Atlantic Microlab, Inc., in Norcross, GA, and are within 0.4% of the calculated values. All intermediate compounds were analyzed but are not reported. Their purity was determined by TLC and ^{1}H NMR. Melting points (mp) were determined on Thomas-Hoover capillary melting point apparatus and are uncorrected.

Hb was generously provided by Drs. John Hess and Victor MacDonald of the U.S. Army Medical Research Detachment, formerly based at the Letterman Laboratories, The Presidio, San Francisco, CA. For oxygen dissociation analyses Hb was further dialyzed against pH 8.6 Tris buffer (50 mM, containing 40 mg of EDTA/L). The Hb was concentrated using a Schleicher and Schuell collodion bag apparatus (Schleicher and Schuell Inc.) with HEPES buffer (50 mM, pH 7.4) as the exchange buffer. The Hb concentration at this point was usually found to be around 35 g % (approximately 5.4 mM) with less than 5% methemoglobin. For all other experiments Hb was dialyzed against 10 mM phosphate buffer, pH 7.0. The concentration of Hb after dialysis was normally around 2 mM. All purified hemoglobin solutions were stored at −82 °C until ready for use. The reagents and buffers were purchased from Sigma Chemical Co., Fisher Scientific Co., and Pharmacia and Research Chemicals, Inc.

Synthesis. (A) Bisaldehyde Alkanes and Xylenes (Classes 1 and 2). Methyl 2-Hydroxy-5-acetalbenzoate (HMAB). A solution of 5-formylsalicylic acid (5-FSA, 5 g, 30 mmol) and concentrated sulfuric acid (4 mL, 71 mmol) in methanol (50 mL) was refluxed for 24 h. The reaction mixture was cooled and evaporated to dryness. The residual product was dissolved in ethyl acetate and washed with an aqueous solution of sodium bicarbonate. The organic layer was dried over $MgSO_4$ and evaporated to give the methyl benzoate, MFSA, as a pale yellow solid of 4.97 g (92%).

Methyl 5-formyl-2-hydroxybenzoate (MFSA) (4.0 g, 22 mmol), ethylene glycol (12 mL, 88 mmol), *p*-toluenesulfonic acid monohydrate (1.20 g), and toluene (100 mL) were charged into a round bottom flask fitted with a Dean Stark apparatus, and the mixture was heated to reflux for 12 h. The reaction mixture was cooled and washed with an aqueous solution of sodium bicarbonate, and the organic layer was dried ($MgSO_4$) and evaporated under reduced pressure. The crude product obtained was purified by flash chromatography using hexane/ethyl acetate (3:1) mixtures as an eluant to give a brown viscous liquid as the desired product: yield 4.34 g (88%); ^{1}H NMR (DMSO-d_6) δ 10.65 (br s, 1H, OH), 7.89 (d, J = 4.1 Hz, 1H, ArH), 7.59 (dd, J = 4.1, 8.2 Hz, 1H, ArH), 7.01 (d, J = 8.2 Hz, 1H, ArH), 5.7 (s, 1H, CH), 3.92−4.1 (m, 4H, CH_2CH_2), 3.9 (s, 3H, CH_3).

Scheme 1

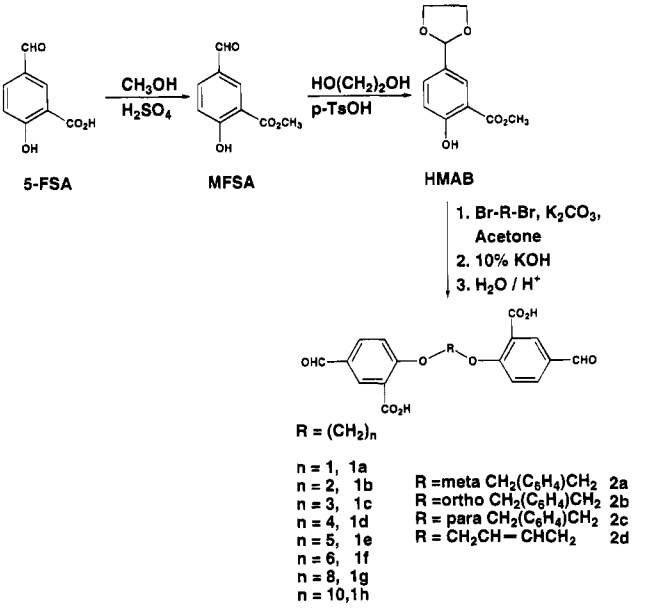

*Bis(2-carboxy-4-formylphenoxy)methane (**1a**).* HMAB (1.0 g, 4.46 mmol), diiodomethane (0.6 g, 2.24 mmol), and powdered potassium carbonate (2.0 g, 14.5 mmol) in dry 2-butanone were refluxed for 24 h. The reaction mixture was filtered while hot, and the solvent was removed under vacuum. The residue was dissolved in ethyl acetate, washed with aqueous sodium hydroxide (0.5 M), followed by water and then brine, and the organic layer was dried ($MgSO_4$) and evaporated under reduced pressure to afford the intermediate diester as a solid. The diester in 10% aqueous potassium hydroxide (30 mL) was refluxed for 1 h, filtered, cooled, and acidified with concentrated hydrochloric acid. The precipitate obtained was filtered and washed thoroughly with water (100 mL) and then with small amounts of diethyl ether. Air-drying of the solid material yielded 0.65 g (**1a**) (85%): mp 175 °C dec; ^{1}H NMR (DMSO-d_6) δ 9.91 (s, 2H, C*H*O), 8.2 (d, J = 4.1 Hz, 2H, ArH), 8.05 (dd, J = 4.1, 8.2 Hz, 2H, ArH), 7.55 (d, J = 8.2 Hz, 2H, ArH), 6.18 (s, 2H, ArOCH_2OAr). Anal. Calcd for $C_{17}H_{12}O_8$: C, 59.30; H, 3.52. Found: C, 59.52; H, 3.55.

The remainder of the molecules in classes 1 and 2 were prepared using the same procedure described for synthesis of **1a** above, with the exception that the appropriate dibromoalkane was substituted for diiodomethane (see Scheme 1).

*1,2-Bis(2-carboxy-4-formylphenoxy)ethane (**1b**):* yield 0.60 g (75%); mp 191 °C dec; ^{1}H NMR (DMSO-d_6) δ 9.91 (s, 2H, CHO), 8.2 (d, J = 4.1 Hz, 2H, ArH), 8.06 (dd, J = 4.1, 8.2 Hz, 2H, ArH), 7.49 (d, J = 8.2 Hz, 2H, ArH), 4.59 (s, 4H, CH_2CH_2). Anal. Calcd for $C_{18}H_{14}O_8$: C, 60.33; H, 3.95. Found: C, 60.64; H, 3.65.

*1,3-Bis(2-carboxy-4-formylphenoxy)propane (**1c**):* yield 0.75 g (90%); mp 192 °C dec; ^{1}H NMR (DMSO-d_6) δ 13.00

(br s, 2H, CO_2H), 9.95 (s, 2H, CHO), 8.2 (d, J = 4.1 Hz, 2H, ArH), 8.05 (dd, J = 4.1, 8.2 Hz, 2H, ArH), 7.39 (d, J = 8.2 Hz, 2H, ArH), 4.4 (t, J = 6.1 Hz, 4H, CH_2), 2.25 (t, J = 6.1 Hz, 2H, CH_2). Anal. Calcd for $C_{19}H_{16}O_8$: C, 61.29; H, 4.33. Found: C, 61.62; H, 4.66.

*1,4-Bis(2-carboxy-4-formylphenoxy)butane (**1d**):* yield 0.82 g (95%); mp 215 °C dec; ^{1}H NMR (DMSO-d_6) δ 12.9 (br, 2H, CO_2H), 9.89 (s, 2H, CHO), 8.15 (d, J = 4.1 Hz, 2H, ArH), 8.05 (dd, J = 4.1, 8.2 Hz, 2H, ArH), 7.39 (d, J = 8.2 Hz, 2H, ArH), 4.2 (br t, 4H, CH_2O), 1.9 (br m, 4H, CH_2). Anal. Calcd for $C_{20}H_{18}O_8$·0.25H_2O: C, 61.46; H, 4.77. Found: C, 61.29; H, 4.69.

*1,5-Bis(2-carboxy-4-formylphenoxy)pentane (**1e**):* yield 0.61 g (68%); mp 231 °C dec; ^{1}H NMR (DMSO-d_6) δ 9.89 (s, 2H, CHO), 8.11 (d, J = 4.1 Hz, 2H, ArH), 7.99 (dd, J = 4.1, 8.2 Hz, 2H, ArH), 7.29 (d, J = 8.2 Hz, 2H, ArH), 4.15 (t, J = 6.1 Hz, 4H, CH_2O), 1.80 (m, 4H, CH_2), 1.60 (m, 2H, CH_2). Anal. Calcd for $C_{21}H_{20}O_8$: C, 62.99; H, 5.04. Found: C, 62.78; H, 5.13.

*1,6-Bis(2-carboxy-4-formylphenoxy)hexane (**1f**):* yield 0.65 g (70%); mp 149 °C dec; ^{1}H NMR (DMSO-d_6) δ 9.90 (s, 2H, CHO), 8.19 (d, J = 4.1 Hz, 2H, ArH), 8.02 (dd, J = 4.1, 8.2 Hz, 2H, ArH), 7.31 (d, J = 8.2 Hz, 2H, ArH), 4.18 (t, J = 6.1 Hz, 4H, CH_2O), 1.75 (m, 4H, CH_2), 1.51 (m, 4H, CH_2). Anal. Calcd for $C_{22}H_{22}O_8$·0.5H_2O: C, 62.41; H, 5.48. Found: C, 62.60; H, 5.42.

*1,8-Bis(2-carboxy-4-formylphenoxy)octane (**1g**):* yield 0.75 g (90%); mp 213 °C dec; ^{1}H NMR (DMSO-d_6) δ 9.89 (s, 2H, CHO), 8.11 (d, J = 4.1 Hz, 2H, ArH), 7.99 (dd, J = 4.1, 8.2 Hz, 2H, ArH), 7.28 (d, J = 8.2 Hz, 2H, ArH), 4.1 (t, J = 6.1 Hz, 4H, CH_2), 1.70 (m, 4H, CH_2), 1.35 (m, 8H, CH_2). Anal. Calcd for $C_{24}H_{26}O_8$: C, 65.14; H, 5.93. Found: C, 64.96; H, 6.00.

*1,10-Bis(2-carboxy-4-formylphenoxy)decane (**1h**):* yield 0.55 g (62%); mp 200 °C dec; ^{1}H NMR (DMSO-d_6) δ 9.90 (s, 2H, CHO), 8.16 (d, J = 4.1 Hz, 2H, ArH), 8.01 (dd, J = 4.1, 8.2 Hz, 2H, ArH), 7.31 (d, J = 8.2 Hz, 2H, ArH), 4.15 (t, J = 6.1 Hz, 4H, CH_2), 1.75 (m, 4H, CH_2), 1.22−1.49 (m, 12H, CH_2). Anal. Calcd for $C_{26}H_{30}O_8$: C, 66.36; H, 6.44. Found: C, 66.18; H, 6.49.

*α,α′-Bis(2-carboxy-4-formylphenoxy)-m-xylene (**2a**):* yield 0.69 g (72%); mp 218−220 °C; ^{1}H NMR (DMSO-d_6) δ 13.1 (br s, 2H, CO_2H), 9.95 (s, 2H, CHO), 8.21 (d, J = 4.1 Hz, 2H, ArH), 8.08 (dd, J = 4.1, 8.2 Hz, 2H, ArH), 7.44 (d, J = 8.2 Hz, 2H, ArH), 7.63−7.5 (m, 4H, ArH), 5.35 (s, 4H, CH_2). Anal. Calcd for $C_{24}H_{18}O_8$·0.5H_2O: C, 65.01; H, 4.32. Found: C, 65.01; H, 4.27.

*α,α′-Bis(2-carboxy-4-formylphenoxy)-o-xylene (**2b**):* yield 0.52 g (54%); mp 200 °C dec; ^{1}H NMR (DMSO-d_6) δ 13.15 (br s, 2H, CO_2H), 9.95 (s, 2H, CHO), 8.22 (d, J = 4.1 Hz, 2H, ArH), 8.08 (dd, J = 4.1, 8.2 Hz, 2H, ArH), 7.49 (d, J = 8.2 Hz, 2H, ArH), 7.7 (m, 2H, ArH), 7.4 (m, 2H, ArH), 5.55 (s, 4H, 2CH_2). Anal. Calcd for $C_{24}H_{18}O_8$: C, 66.36; H, 4.18. Found: C, 66.35; H, 4.22.

*α,α′-Bis(2-carboxy-4-formylphenoxy)-p-xylene (**2c**):* yield 0.98 g (96%); mp 220−222 °C; ^{1}H NMR (DMSO-d_6) δ 13.05 (br s, 2H, CO_2H), 9.95 (s, 2H, CHO), 8.21 (d, J = 4.1 Hz, 2H, ArH), 8.05 (dd, J = 4.1, 8.2 Hz, 2H, ArH), 7.43 (d, J = 8.2 Hz, 2H, ArH), 7.55 (s, 4H, ArH), 5.35 (s, 4H, 2CH_2). Anal. Calcd for $C_{24}H_{18}O_8$·0.75H_2O: C, 64.36; H, 4.36. Found: C, 64.29; H, 4.24.

*1,4-Bis(2-carboxy-4-formylphenoxy)-2-butene (**2d**):* yield 0.79 g (92%); mp 211−213 °C; ^{1}H NMR (DMSO-d_6) δ 12.35 (br s, 2H, CO_2H), 9.95 (s, 2H, CHO), 8.25 (d, J = 4.1 Hz, 2H, ArH), 8.09 (dd, J = 4.1, 8.2 Hz, 2H, ArH), 7.4 (d, J = 8.2 Hz, 2H, ArH), 6.25 (br s, 2H, olefinic protons), 4.85 (br s, 4H, CH_2). Anal. Calcd for $C_{20}H_{16}O_8$·0.5H_2O: C, 61.07; H, 4.36. Found: C, 61.31; H, 4.30.

Scheme 2

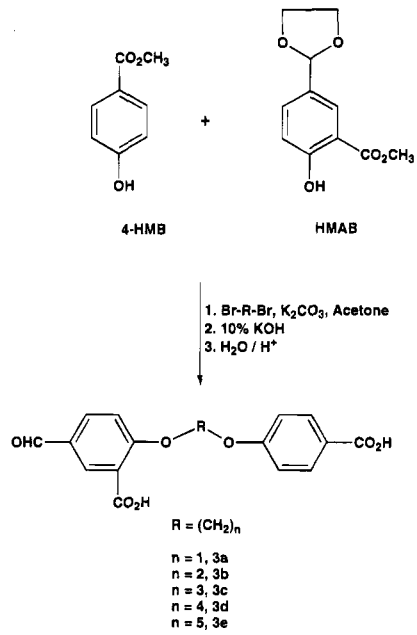

*1-(2-Carboxy-4-formylphenoxy)-1-(4-carboxyphenoxy)-methane (**3a**).* A mixture of HMAB (1.0 g, 4.46 mmol), methyl 4-hydroxybenzoate (HMB, Aldrich) (0.68 g, 4.46 mmol), diiodomethane (1.2 g, 4.48 mmol), and powdered potassium carbonate (4.0 g, 29 mmol) in dry acetone was refluxed for 24 h. The reaction mixture was filtered and the solvent was removed under vacuum. The residue was flash chromatographed using hexane/ethyl acetate (5:1) as an eluant to obtain the intermediate diester. A suspension of the diester and 10% aqueous potassium hydroxide (50 mL) was refluxed for 1 h; the reaction mixture was filtered, cooled, and acidified with concentrated hydrochloric acid. The precipitate was filtered, washed thoroughly with water (100 mL), and air-dried to yield 1.05 g (74.7%) of the title compound (**3a**): mp 202−204 °C dec; ^{1}H NMR (DMSO-d_6) δ 12.85 (br s, 2H, CO_2H), 9.9 (s, 1H, CHO), 8.2 (d, J = 4.1 Hz, 1H, ArH), 8.05 (dd, J = 4.1, 8.2 Hz, 1H, ArH), 7.9 (d, J = 8.2 Hz, 2H, ArH), 7.36 (d, J = 10.2 Hz, 1H, ArH), 7.01 (d, J = 10.2 Hz, 2H, ArH), 6.18 (s, 2H, CH_2). Anal. Calcd for $C_{16}H_{11}O_7$: C, 60.95; H, 3.52. Found: C, 60.86; H, 3.55.

The remainder of the molecules in class 3 were prepared using the same procedure described for synthesis of **3a** above, with the exception that the appropriate dibromoalkane was substituted for diiodomethane (see Scheme 2).

*1-(2-Carboxy-4-formylphenoxy)-2-(4-carboxyphenoxy)-ethane (**3b**):* yield 1.12 g (76.3%); mp 221−223 °C dec; ^{1}H NMR (DMSO-d_6) δ 12.85 (br s, 2H, CO_2H), 9.9 (s, 1H, CHO), 8.2 (d, J = 4.1 Hz, 1H, ArH), 8.05 (dd, J = 4.1, 8.2 Hz, 1H, ArH), 7.9 (d, J = 8.2 Hz, 2H, ArH), 7.36 (d, J = 10.2 Hz, 1H, ArH), 7.01 (d, J = 10.2 Hz, 2H, ArH), 4.59 (s, 4H, CH_2CH_2). Anal. Calcd for $C_{17}H_{13}O_7$: C, 62.00; H, 3.99. Found: C, 62.08; H, 4.10.

*1-(2-Carboxy-4-formylphenoxy)-3-(4-carboxyphenoxy)propane (**3c**):* yield 1.18 g (77%); mp 211−213 °C dec; ^{1}H

Scheme 3

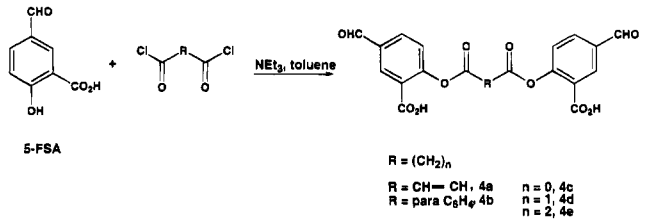

NMR (DMSO-d_6) δ 12.85 (br s, 2H, CO_2H), 9.9 (s, 1H, CHO), 8.2 (d, J = 4.1 Hz, 1H, ArH), 8.05 (dd, J = 4.1, 8.2 Hz, 1H, ArH), 7.9 (d, J = 8.2 Hz, 2H, ArH), 7.36 (d, J = 10.1 Hz, 1H, ArH), 7.01 (d, J = 10.1 Hz, 2H, ArH), 4.4 (t, J = 6.1 Hz, 4H, CH_2), 2.25 (t, J = 6.1 Hz, 2H, CH_2). Anal. Calcd for $C_{18}H_{15}O_7$: C, 62.97; H, 4.41. Found: C, 62.92; H, 4.33.

*1-(2-Carboxy-4-formylphenoxy)-4-(4-carboxyphenoxy)butane (**3d**):* yield 1.31 g (82%); mp 185 °C dec; ^{1}H NMR (DMSO-d_6) δ 12.85 (br s, 2H, CO_2H), 9.9 (s, 1H, CHO), 8.2 (d, J = 4.1 Hz, 1H, ArH), 8.05 (dd, J = 4.1, 8.2 Hz, 1H, ArH), 7.9 (d, J = 8.2 Hz, 2H, ArH), 7.36 (d, J = 10.1 Hz, 1H, ArH), 7.01 (d, J = 10.1 Hz, 2H, ArH), 4.25 (t, J = 7.1 Hz, 2H, CH_2O), 4.11 (t, J = 7.1 Hz, 2H, CH_2O), 1.95 (m, 4H, CH_2). Anal. Calcd for $C_{19}H_{18}O_7 \cdot H_2O$: C, 60.64; H, 5.36. Found: C, 60.76; H, 5.11.

*1-(2-Carboxy-4-formylphenoxy)-5-(4-carboxyphenoxy)pentane (**3e**):* yield 1.23 g (82%); mp 198 °C dec; ^{1}H NMR (DMSO-d_6) δ 12.85 (br s, 2H, CO_2H), 9.9 (s, 1H, CHO), 8.2 (d, J = 4.1 Hz, 1H, ArH), 8.05 (dd, J = 4.1, 8.2 Hz, 1H, ArH), 7.9 (d, J = 8.2 Hz, 2H, ArH), 7.36 (d, J = 10.2 Hz, 1H, ArH), 7.01 (d, J = 10.2 Hz, 2H, ArH), 4.15 (t, J = 7.1 Hz, 4H, CH_2O), 1.80 (m, 4H, CH_2), 1.60 (m, 2H, CH_2). Anal. Calcd for $C_{20}H_{20}O_7$: C, 64.50; H, 5.42. Found: C, 64.53; H, 5.39.

*(B) Bisaldehyde Bisesters (Class 4). Bis(2-carboxy-4-formylphenyl)fumarate (**4a**).* A solution of 5-formylsalicylic acid (5-FSA, 1.66 g, 10 mmol) and fumaryl chloride (1.53 g, 10 mmol) in dry toluene (50 mL) was refluxed for 24 h, and the solvent was removed in vacuo. The residue was dissolved in acetone (30 mL), and the product was precipitated by the addition of absolute ethanol. Recrystallization from acetone yielded the pure product: 1.32 g (64%); mp 180−182 °C; ^{1}H NMR (DMSO-d_6) δ 10.1 (s, 2H, CHO), 8.53 (d, J = 4.1 Hz, 2H, ArH), 8.23 (dd, J = 4.1, 8.2 Hz, 2H, ArH), 7.63 (d, J = 8.2 Hz, 2H, ArH), 7.28 (br s, 2H, olefinic protons). Anal. Calcd for $C_{20}H_{12}O_{10} \cdot H_2O$: C, 55.82; H, 3.28. Found: C, 55.70; H, 3.27.

The following compounds were synthesized with the same procedure as described for **4a** (see Scheme 3).

*Bis(2-carboxy-4-formylphenyl) Terephthalate (**4b**):* yield 3.20 g (69.2%); mp 209−211 °C; ^{1}H NMR (DMSO-d_6) δ 9.91 (s, 2H, CHO), 8.53 (d, J = 4.1 Hz, 2H, ArH), 8.23 (dd, J = 4.1, 8.2 Hz, 2H, ArH), 7.63 (d, J = 8.2 Hz, 2H, ArH), 7.55 (q, J = 8.9 Hz, 4H, ArH). Anal. Calcd for $C_{24}H_{14}O_{10}$: C, 62.34; H, 3.06. Found: C, 62.42; H, 3.19.

*Bis(2-carboxy-4-formylphenyl) Oxalate (**4c**):* yield 1.15 g (59.5%); mp 182−184 °C; ^{1}H NMR (acetone-d_6) δ 13.01 (br s, 2H, CO_2H), 10.1 (s, 2H, CHO), 8.52 (d, J = 4.1 Hz, 2H, ArH), 8.22 (dd, J = 4.1, 8.2 Hz, 2H, ArH), 7.63 (d, J = 8.2 Hz, 2H, ArH). Anal. Calcd for $C_{18}H_{10}O_{10}$: C, 55.97; H, 2.62. Found: C, 55.84; H, 2.57.

Table 1: Effect of Compounds on the Oxygen Affinity of Hemoglobin[a]

compound	P_{50}	ΔP_{50}	compound	P_{50}	ΔP_{50}
classes 1 and 2			class 3		
av control	21.9 ± 0.5		av control	22.0 ± 0.0	
1a	51.0 ± 0.6	29.0	**3a**	39.0 ± 0.0	17.0
1b	46.0 ± 0.0	24.0	**3b**	38.0 ± 1.6	16.0
1c	44.0 ± 0.6	22.0	**3c**	35.0 ± 1.6	13.0
1d	42.0 ± 0.6	20.0	**3d**	33.0 ± 0.6	11.0
1e	33.0 ± 1.5	11.0	**3e**	33.3 ± 0.3	11.3
1f	39.0 ± 1.7	16.0	class 4		
1g	37.0 ± 0.0	15.0	av control	20.4 ± 0.6	
1h	33.0 ± 0.6	11.0	**4a**	14.0 ± 0.6	−6.0
2a	4.5 ± 0.0	4.5	**4b**	16.0 ± 1.6	−4.0
2b	9.5 ± 0.6	9.5	**4c**	19.5 ± 0.3	−1.5
2c	2.5 ± 0.6	2.5	**4d**	19.0 ± 0.0	−2.0
2c	40.0 ± 0.6	18.0	**4e**	14.5 ± 0.3	−5.5

[a] All studies were performed with 2.7 mM hemoglobin in the presence of 10 mM drug. Compounds were dissolved in 50 mM HEPES buffer (pH 7.4) containing 2 molar equiv of sodium bicarbonate and incubated with hemoglobin A for 30 min at room temperature, and oxygen equilibrium analysis was performed as described. P_{50} values represent the oxygen pressure (mmHg) at which drug-treated hemoglobin is 50% oxygen saturated and are expressed as the mean ± SEM for three separate measurements. ΔP_{50} values represent the mean difference between the vehicle control and drug-treated samples.

*Bis(2-carboxy-4-formylphenyl) Malonate (**4d**):* yield 1.55 g (81%); mp 205−207 °C dec; ^{1}H NMR (acetone-d_6) δ 12.89 (br s, 2H, CO_2H), 9.91 (s, 2H, CHO), 8.52 (d, J = 4.1 Hz, 2H, ArH), 8.23 (dd, J = 4.1, 8.2 Hz, 2H, ArH), 7.63 (d, J = 8.2 Hz, 2H, ArH), 6.01 (s, 2H, CH_2). Anal. Calcd for $C_{19}H_{12}O_{10}$: C, 54.00; H, 3.03. Found: C, 54.12; H, 2.98.

*Bis(2-carboxy-4-formylphenyl) Succinate (**4e**):* yield 4.6 g (64%); mp 218−220 °C; ^{1}H NMR (DMSO-d_6) δ 9.89 (s, 2H, CHO), 8.53 (d, J = 4.1 Hz, 2H, ArH), 8.23 (dd, J = 4.1, 8.2 Hz, 2H, ArH), 7.63 (d, J = 8.2 Hz, 2H, ArH), 2.9 (s, 4H, CH_2). Anal. Calcd for $C_{20}H_{14}O_{10}$: C, 57.93; H, 3.41. Found: C, 57.76; H, 3.38.

Oxygen Dissociation Curves. In Richmond, oxygen dissociation curves were recorded on an Aminco Hem-O-Scan oxygen dissociation analyzer (Travenol Laboratories) as previously described (Randad et al., 1991). All diacids were dissolved in 50 mM HEPES buffer, pH 7.4, using 2 equiv of sodium bicarbonate to prepare 20 mM drug solution. The Hb (5.4 mM, in HEPES, pH 7.4) and the test compounds (20 mM) were mixed in 1:1 volume ratio (50 μL of compound solution) to give final concentrations of 2.7 and 10 mM, respectively (a molar ratio of test compound to hemoglobin of approximately 4:1). A control experiment was prepared by the addition of 50 μL of Hb to 50 μL of HEPES buffer. The mixture was incubated at room temperature for 30 min before the oxygen dissociation curves were run. The P_{50} values are given in Table 1.

In Paris, T-state crystals of reacted and reduced allosteric effector−Hb complexes were dissolved in buffer at pH 7.2 at 25 °C. The composition of the buffer system was 100 mM NaCl and 50 mM bis-Tris. Catalase (20 μg/mL) and 50 μM EDTA were added to limit oxidation of the hemes during the 45−60 min of the recordings. Measurements of the oxygen dissociation curves were performed using a Hemox analyzer (TCS Medical Products) as described in detail previously (Abraham et al., 1992b; Kister et al., 1987). The P_{50} and n_{50} values were calculated by linear regression analysis from data points comprised between 40% and 60% oxygen saturation.

Table 2: Crystallographic Data[a]

compd added to HbA	cell dimensions				d_{lim}[b]	R_{merge},[c]	R_{d-n}[d]
	a, Å	b, Å	c, Å	β, deg	Å	%	%
1a,[e] $n = 1$	63.17	83.55	53.82	99.47	1.94	5.6	9.3
1a,[f] $n = 1$	63.22	83.64	53.93	99.57	1.94	5.7	11.5
1b,[e] $n = 2$	63.17	83.51	53.77	99.42	1.94	7.2	10.5
1c,[e] $n = 3$	63.28	83.55	53.81	99.53	1.94	4.5	9.3
1c,[f] $n = 3$	63.28	83.49	53.87	99.73	1.94	5.7	10.7
1d,[e] $n = 4$	63.24	83.40	53.83	99.38	1.94	5.7	9.5
1e,[e] $n = 5$	63.24	83.55	53.83	99.49	1.94	6.1	11.2
2a,[e] R = *m*-xylene	63.24	83.51	53.90	99.40	1.94	5.3	10.4
3d,[e] $n = 4$	63.27	83.48	53.83	99.45	1.94	7.1	11.6
4a,[e] R = ethene	63.43	83.77	53.82	99.35	1.94	6.2	10.5

[a] Crystals obtained from HbA tetramer to compound ratio of 1:5. [b] d_{lim} is the radius of the limiting sphere in which data were collected. [c] R_{merge} is the consistency of equivalent reflection between the entire R-axis IIC image plate data set; $R_{merge} = \sum\sum|F^2(I)/G(I) - \langle F^2(h)\rangle|/\sum\sum F^2(I)/G(I)$. [d] R_{d-n} is the agreement factor of structure amplitudes between native and derivative data; $R_{d-n} = \sum_{hkl}(|F_d| - |F_n|)/\sum_{hkl}|F_d|$. [e] Data set from crystals obtained from incubation and reduction of the aldehydic compounds and HbA in air. [f] Data set from crystals obtained from incubation and reduction of the aldehydic compounds and HbA under anaerobic conditions.

Table 3: Sequencing Data Summarized in Terms of the Number of Chains Going through the Edman Chemistry

compd	predicted first cycle Val per chain,[a] pmol	actual first cycle Val, pmol	equiv (no. of chains seq)
bisaldehyde alkanes and xylene			
1a, $N = 1$	417	191	0.45 (<1 chain)
1b, $N = 2$	208	77	0.37 (<1 chain)
1c, $N = 3$	465	212	0.45 (<1 chain)
1d, $N = 4$	207	50	0.25 (≪1 chain)
1e, $N = 5$	1028	271	0.26 (≪1 chain)
1f, $N = 6$	429	389	0.91 (1 chain)
2a	5620	5538	0.99 (1 chain)
monoaldehyde bisacid			
3d, $N = 4$	389	336	0.86 (1 chain)
bisaldehyde bisester			
4a	387	61	0.15 (≪1 chain)

[a] Predicted first cycle yield of Val is based on the sum of the yield of His_β (second cycle), Leu_β (third cycle), and Ala_α (fifth cycle) divided by 4 assuming that these latter residues represent four sequencing chains. N represents the number of carbons in the chain separating the two phenyl rings. no. of chains sequencing = actual first cycle Val/predicted first cycle Val.

Reaction Conditions and Crystallization. Reaction and reduction of the aldehyde−Hb complexes, crystal preparations, and X-ray data collection were carried out with slight modifications according to the procedures of Wireko and Abraham (1991). To assure that high salt concentrations used for crystal growth did not influence binding, all effector aldehydes were incubated and reduced *in air* under low salt conditions. Freshly prepared solutions of the compounds in 50 mM potassium phosphate buffer, pH 7.2, were incubated with oxy-Hb (dialyzed in 10 mM phosphate buffer, pH 7.0) for at least 24 h with an effector to Hb (tetramer) molar ratio of 5/1. An excess of effector was used to obtain a more complete reaction with Hb and is close to the standard ratio (4/1) that we have used to compare allosteric potency among different effectors (Randad et al., 1991). Reduction of the unstable Schiff base linkage to produce an alkylamine covalent bond is necessary to observe X-ray binding (Manning & Manning, 1988; Wireko & Abraham, 1991). Sodium cyanoborohydride in 50 mM phosphate buffer, pH 7.2, was added in 10−50-fold molar excess of Hb tetramer to reduce the Schiff base adduct for at least 3 h. The deoxygenated Hb−effector complexes were set up for crystallization following the procedures described by Perutz (1968) using ammonium sulfate. X-ray quality crystals for all complexes were obtained from 3 to 7 days. Crystals of **1a**− and **1c**−Hb complexes incubated and reduced under deoxygenated conditions were also grown and diffracted.

X-ray Data Collection and Difference Maps. X-ray diffraction data for the complexed allosteric effectors were obtained with a Rigaku RU-200 rotating anode equipped with an R-axis IIC image plate system to a resolution of 1.94 Å. Crystals of 0.2−0.5 mm linear dimensions were used. Data reduction, structure solution, and calculation of Fourier difference electron density maps were calculated as previously described (Abraham et al., 1995b; Wireko & Abraham, 1991). Crystallographic data are summarized in Table 2. Raw data sets were also processed as already described (Wireko & Abraham, 1991) or with the Rigaku R-axis II software programs (Abraham et al., 1995b). Difference electron density maps were computed from the $[F_{obs(deriv)} - F_{obs(native)}]$ amplitudes at 4.0, 3.5, 3.0, and 2.0 Å resolutions, where $F_{obs(deriv)}$ is the observed structure factors of the aldehyde−Hb complexes and $F_{obs(native)}$ is the observed structure factors from the previously determined structure of native T-state Hb (Fermi et al., 1984). Electron density maps calculated at all four resolutions produced overlapping contours for each effector binding site with identical fit of the molecule to the density at the four resolutions. The noise level in the difference map increased with the increase in resolution (the 2.0 Å map had the most noise). The agreement factor for the structure amplitudes between native and derivative data (R_{d-n}) is reported in Table 2 at 2.0 Å resolution. All figures and diagrams illustrating the difference electron density maps utilized 3.0 Å resolution density (the same fit was obtained for the 3.5, 3.0, and 2.0 Å maps). The maps illustrated were contoured at 3.0−4.0σ, where σ is the rms electron density in the unit cell. $[2F_{obs(deriv)} - F_{obs(native)}]$ difference electron density maps were also calculated at the above resolutions and contoured at 1.0σ to confirm the drug positions. Models of the compounds created with MMOD12 (Still et al., 1989) and minimized with the MM2 force field were fit to the electron density using FRODO (Evans, 1985) on an Evans and Sutherland PS390 graphic station.[2]

The geometry around a Schiff base double bond is trigonal planar while the geometries around a reduced Schiff base nitrogen and carbon are tetrahedral. All structural comparisons in this work are with the reduced Schiff base derivatized hemoglobins. High-resolution refinement of a selected number of the derivatized hemoglobins in both the T- and R-states is underway and will be presented elsewhere.

Characterization of the Crystals Used for the Diffraction Studies: Sequencing. Sequencing studies were conducted to confirm the X-ray difference map indication of reaction at the N-terminal Val residues. Single crystals of the derivatized T-state hemoglobin selected from the batches used for X-ray studies were dissolved in approximately 200 μL of doubly distilled water. For each sample, 50 μL was diluted

[2] Coordinates for any of the reported structures in this paper can be obtained from the corresponding author.

1:1 in 0.2% (v/v) trifluoroacetic acid in water and the entire sample applied to a prepared sequencing cartridge. Automated sequence analysis was done on five cycles for each sample; the picomoles of each phenylthiohydantoin- (PTH-) amino acid detected was tabulated to determine cycle yields. The secondary amine produced by the reduction of the Schiff base double bond appears to produce a new PTH-amino acid derivative with different retention times for the non-cross-linked samples as discussed in the accompanying paper (Abraham et al., 1995b). The remainder of the α and β chains sequenced in the normal ratios expected for the two different subunits. The average chains sequencing were calculated from a comparison of the predicted first cycle yield of Val based on the average of the picomole yields of His_β (second cycle), Leu_β (third cycle), and Ala_α (fifth cycle) and are presented in Table 3.

Isoelectric focusing electrophoresis was also employed (4 °C) to analyze crystals used for the diffraction studies.

RESULTS

Design. 5-Formylsalicylic acid (5-FSA) and substituted aromatic phenoxy ethers (2-BF and 2-PEF) have been shown to bind to Val 1α diagonally and parallel to the molecular 2-fold axis (Abraham et al., 1995b), similar but opposite in direction to antisickling aldehyde 12C79 (Wireko & Abraham, 1991). The crystal structures of 2-BF and 2-PEF showed that the *para* positions of their terminal aromatic rings were pointed toward Lys 99α. It was envisioned that the addition of a second aldehyde group linked by a chain with the proper length at the *para* position might form a second Schiff base interaction with the opposite Lys 99α.

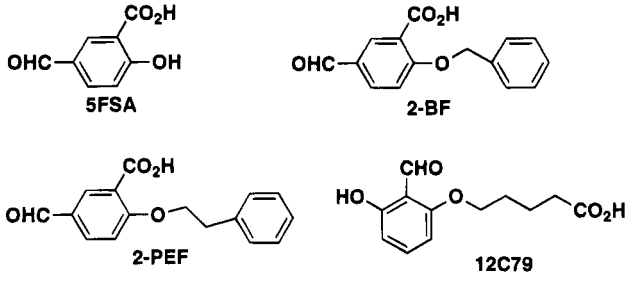

Therefore, the coordinates for 5-FSA, 2-BF, and 2-PEF were employed as starting points, and a series of bisaldehyde molecules (classes 1 and 2) were designed with varying lengths to stretch from the N-terminal Val nitrogen of one α subunit to Lys 99α of the opposite subunit. The bisaldehydes with a *n*-propyl bridge (**1c**) had the ideal length to interact as proposed with the deoxy-Hb (16.0 Å between aldehyde oxygens, Figure 1a). If classes 1 and 2 bind as designed, cross-linking Val 1α with Lys 99α of the opposite subunit, the variable length of the intervening chain could demonstrate different allosteric properties. Lys 99α has been identified as a key residue in shifting the allosteric equilibrium toward the T-state (Abraham et al., 1992a, 1995a; Wireko et al., 1991).

When the same derivatives were modeled into the central water cavity to bind to both Val 1α N-terminal nitrogens in a horizontal manner, similar to the designed binding mode for 12C79 (Beddell et al., 1984), the monoalkyl derivative (**1a**, $n = 1$) had the ideal length to bind to oxy-Hb and **1b** ($n = 2$) to deoxy-Hb (Figure 1b). However, the differences in distances required to cross-link Val $1\alpha_1$ with Val $1\alpha_2$ vs

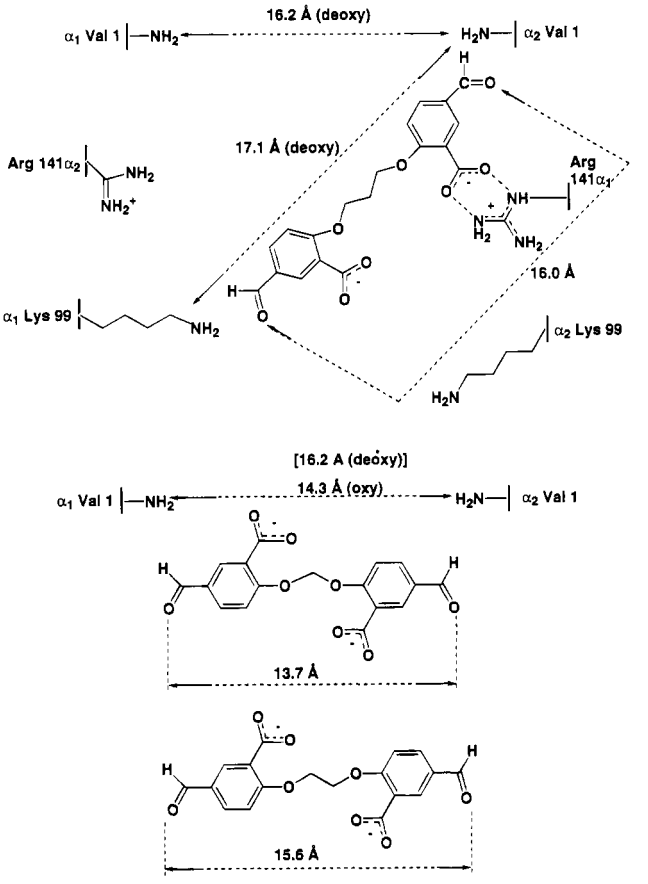

FIGURE 1: (a, top) This figure shows the proposed binding of compound **1c** to deoxy-Hb. Molecule **1c** has the dimensions (16.0 Å) to cross-link Val 1α N-terminal nitrogens (16.2 Å) or Val $1\alpha_2$ with Lys $99\alpha_1$ (17.1 Å). The distances are measured (arrows) from the effector oxygens and hemoglobin N-terminal nitrogens since the N-terminal nitrogens occupy the same space as the aldehyde oxygens once a Schiff base linkage is formed. (b, bottom) This figure shows the differences in distance between the N-terminal Val 1α nitrogens in oxy (14.3 Å) and deoxy (16.2 Å) Hb. Compound **1a** would best fit oxy-Hb (13.7 Å) and compound **1b** (15.6 Å) deoxy-Hb. However, none of the distances in (a) or (b) are large enough to discriminate between compounds **1a**, **1b**, or **1c** since the protein side chains can move to accommodate such small differences.

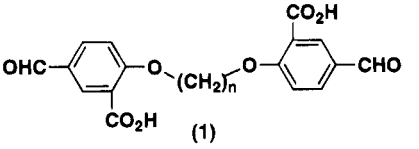

Bis(2-Carboxy-4-Formylphenoxy)-Alkanes

n = 1, 1a	n = 5, 1e
n = 2, 1b	n = 6, 1f
n = 3, 1c	n = 8, 1g
n = 4, 1d	n = 10, 1h

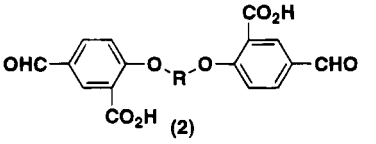

Bis(2-Carboxy-4-Formylphenoxy)-Xylenes

R = meta $CH_2(C_6H)_4CH_2$, 2a
R = ortho $CH_2(C_6H)_4CH_2$, 2b
R = para $CH_2(C_6H)_4CH_2$, 2c
R = $CH_2CH{=}CHCH_2$ 2d

Val $1\alpha_1$ with Lys $99\alpha_2$ (in either the T- or R-state) are too

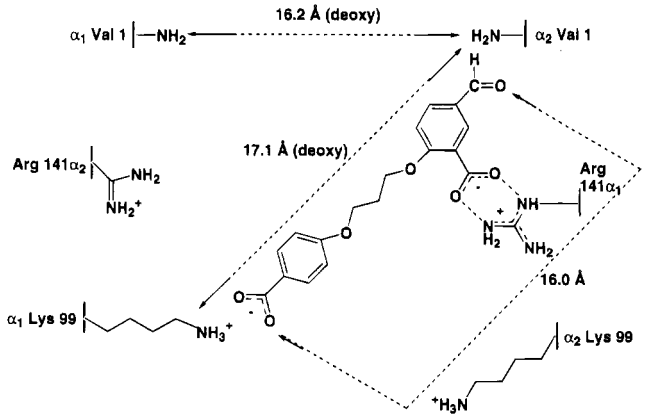

FIGURE 2: This figure shows the binding of compound **3c** to the Val $1\alpha_2$–Lys $99\alpha_1$ site in deoxy-Hb. The fit is similar to the fit of compound **1c** in Figure 1a except that a salt bridge is formed with Lys $99\alpha_1$ instead of a covalent bond.

close to be discriminatory. Movements within the protein and the allosteric effector can accommodate either binding mode. Initially, we believed that nucleophilic attack by both Val 1α N-terminal nitrogens might take preference over cross-linking Val 1α with Lys 99α of the opposite subunit due to the greater number of unprotonated N-terminal amino nitrogens ($pK_A \cong 7.5$ vs $\cong 10.5$ for Lys). However, the pK_A of Lys 99α may be lower than expected due to repulsion of positive charges in close proximity. Both Lys 99α ammonium ions are too close to assume a symmetry-related conformation in the Hb central water cavity (Fermi et al., 1984). If so, this would make them more attractive as nucleophiles.

The monoaldehyde bisacids (class 3) are directly related to the bisaldehydes with the only difference being the exchange of one of the aldehyde groups by an acid. We assumed that the primary site of reaction of the monoaldehyde bisacids of class 3 would be at the N-terminal Val 1α as found in our previous monoaldehyde studies (Abraham et al., 1995b). The acid replacement of the terminal aldehyde was modeled to form a salt bridge with the ammonium ion of Lys 99α of the opposite subunit (Figure 2). We envisioned that this binding mode would take preference to one that stretches across the 2-fold symmetry axis since the unprotonated N-terminal Val nitrogens (lower pK_A) would discourage salt bridge formation.

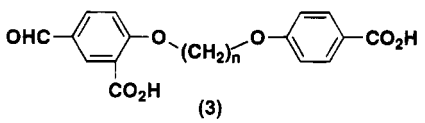

(3)

(2-Carboxy-4-Formylphenoxy)-(4-Carboxyphenoxy)-Alkanes

n = 1, 3a **n = 4, 3d**
n = 2, 3b **n = 5, 3e**
n = 3, 3c

The final series of molecules modeled, the bisaldehyde bisesters (class 4), were designed to cross-link the Val 1α residues via Schiff base formation of the aldehyde groups and to test the reactivity of the effector aldehyde vs the ester group on Hb. Since the class 4 molecules would be reacted and reduced under oxy conditions, the ester groups could react at the β subunit cleft with the β Lys 82 residues as was found with bis(3,5-dibromosalicyl) fumarate when incubated in air (Chatterjee et al., 1982). Another possible

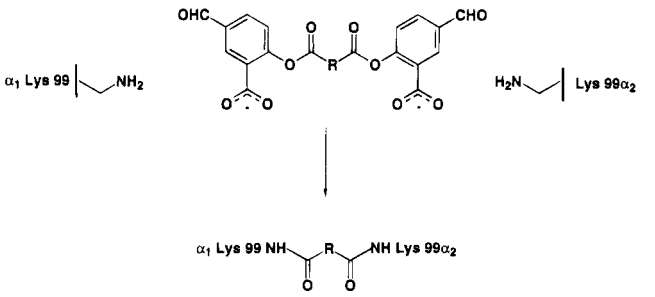

FIGURE 3: This figure illustrates the possible binding (cross-linking) of class 4 molecules by Lys 99α residues in deoxy-Hb.

site of interaction, under deoxy conditions, would involve cross-linking Lys 99α (Figure 3) as found with bis(3,5-dibromosalicyl) fumarate when incubated in the T-state.

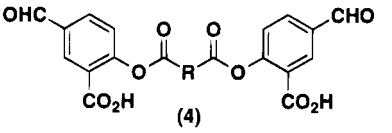

(4)

R = CH=CH 4a
R = para C_6H_4 4b
R = 0 4c
R = CH_2 4d
R = CH_2CH_2 4e

Bis(2-Carboxy-4-Formylphenyl)-Esters

Synthesis of Compounds. The various bisaldehyde alkanes and xylenes (classes 1 and 2) were synthesized as shown in Scheme 1. The monoaldehyde bisacids (**3**) were synthesized according to Scheme 2. Scheme 3 outlines the synthesis of the bisaldehyde bisesters (**4**). Synthesis of the desired molecules was accomplished without difficulty.

X-ray Crystallography and Solution Oxygen Equilibrium Studies. The X-ray diffraction difference maps exhibited well-defined density for the binding of symmetry-related pairs of bisaldehydes at the α and only small difference density peaks at the β N-terminal Val nitrogens. Therefore, the occupancy of reacted molecules at the β subunits was initially assumed to be low or the effector disordered. All primary and secondary binding sites appeared at the highest density levels, well above background ($3-4\sigma$).

(A) Bis(2-carboxy-4-formylphenoxy)-n-alkanes (1). Difference electron density maps were obtained with five bis-(2-carboxy-4-formylphenoxy)-*n*-alkanes: $n = 1$ (**1a**), $n = 2$ (**1b**), $n = 3$ (**1c**), $n = 4$ (**1d**), and $n = 5$ (**1e**). The bis(2-carboxy-4-formylphenoxy)-*n*-alkanes with $n = 2-4$ were found to bind in symmetry-related pairs to Val 1α of one subunit and Lys 99α of the opposite subunit as modeled in Figure 1a. Figure 4 is a representative fit of one of these (**1c**) to the electron density. Positive and negative difference density was observed near protein side chains that interact with the alkyl bisaldehydes, indicating that these residues move: Val 1α, Arg 141α, Thr 134α, Lys 127α, Ala 130α, Pro 95α, Val 96α, Lys 99α, and Thr 137α. The difference map for **1e** ($n = 5$) only revealed density near Val 1α and Lys 99α, and no intervening density could be found to fit the molecule, indicating disorder in the bridging chain as it lengthens. Close contacts between the effectors **1b**, **1c**, and **1d** and protein residues are shown in Figure 5a–c.

The fitting of $n = 1$ (**1a**) to the electron density is shown in Figure 6. The single methylene bridge in **1a** is not quite long enough to position an aldehyde group near Lys 99α after the opposite aldehyde group has formed a Schiff base with Val 1α. Electron density around and near Lys 99α indicates that it probably moves to form a Schiff base interaction. The *m*-carboxylate of **1a** forms the same

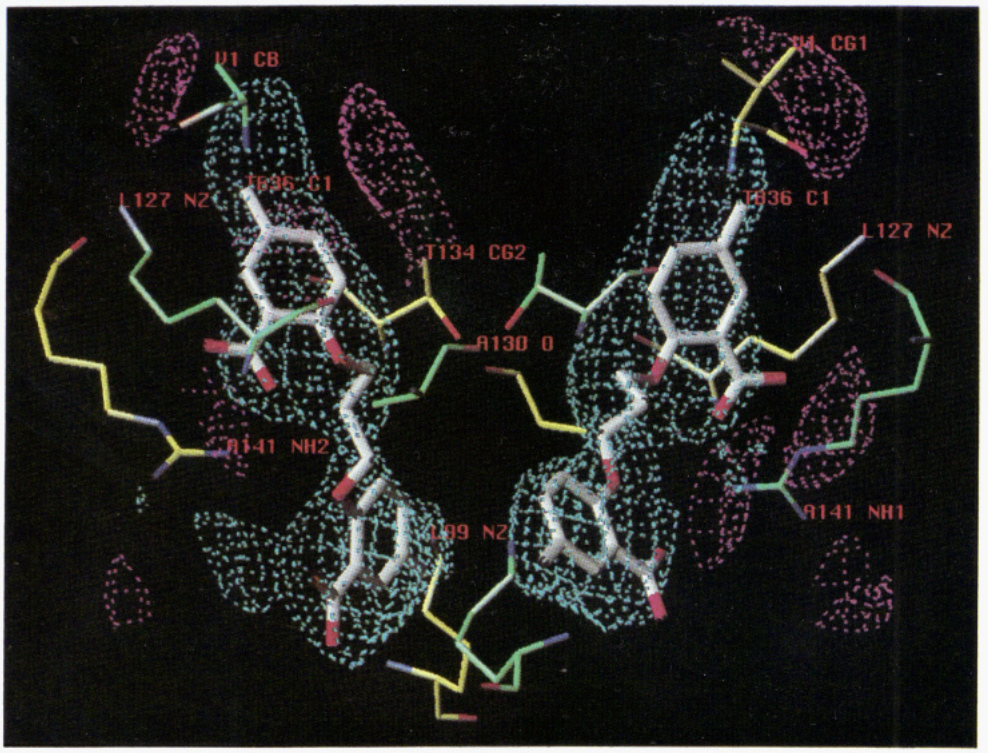

FIGURE 4: This figure shows the fit of symmetry-related pairs of **1c** molecules (white) fit to the electron density. The α_1 subunit residues are in green and the α_2 subunits are in yellow. Positive density (cyan) surrounds the entire molecule. One aldehyde carbon is covalently attached to the N-terminal Val 1α nitrogen, and the second aldehyde is bound to the opposite chain Lys 99 ammonium ion (Val $1\alpha_1$, upper left, in green with Lys $99\alpha_2$, bottom left center, in yellow and Val $1\alpha_2$, upper right, in yellow with Lys $99\alpha_1$, bottom right center, in green). The aldehyde that is linked to the Lys ammonium ion is buried in the back of the density. Positive (cyan) and negative (magenta) difference density was observed near protein side chains that interact with the alkyl bisaldehydes, indicating that the following residues move: Val 1α, Arg 141α, Thr 134α, Lys 127α, Ala 130α, Pro 95α, Val 96α, Lys 99α, and Thr 137α.

bidentate hydrogen bond and salt bridge with the guanidinium ion of Arg 141α of the opposite subunit while the other carboxylate interacts with Thr 134 α of the same subunit (close contacts are shown in Figure 5d). The fitting of **1a** to the density also indicates that symmetry-related molecules are too close to one another near the terminal phenyl ring carboxylates (Figure 6). This would mean that one molecule is oriented in the same fashion as observed for the $n = 2-4$ chains, while the second molecule has the terminal phenyl ring disordered to relieve the steric strain. The lack of density near the top of the phenyl rings supports this interpretation. The region near the point of attachment to Lys 99α is ordered, and there is density for each molecule at this juncture (Figure 6).

Table 1 shows oxygen equilibrium shifts (ΔP_{50} values) determined in the presence of the class 1 bisaldehyde alkanes effectors when incubated in air with Hb (before reduction of the Schiff base linkage). Effectors with the shortest bridges exhibited much stronger right shifts than those observed for the monoaldehydes (Abraham et al., 1995b). The most active effector complex was **1a**, with a single methylene bridge ($n = 1$). The shift in P_{50} consistently increases with decreasing chain length. This indicates that the *tighter* the α chains are held together, the *greater* the degree of *constraint* on the T-state structure and the greater the shift in the allosteric equilibrium. A similar suggestion has been made for effectors bound to various β chain sites where the distance between the cross-linking groups is thought to be related to the degree of shift in the oxygen equilibrium (Kluger et al., 1994).

(B) Bis(2-carboxy-4-formylphenoxy)xylenes (2). Three bis(2-carboxy-4-formylphenoxy)xylenes, *meta* (**2a**), *para* (**2c**), and *ortho* (**2b**), were synthesized by replacing the flexible aliphatic chain (with higher entropy for binding) by an aromatic linkage that is less flexible (with lower entropy). The *o*- and *p*-xylenes were only slightly soluble, so only the crystal structure of bis(2-carboxy-4-formylphenoxy)-*m*-xylene (**2a**) was performed. The difference electron density map revealed that the *m*-xylene bisaldehyde also cross-linked Val 1α with Lys 99α of the opposite subunit. Close contacts with the protein are shown in Figure 5e. Table 1 indicates that the bisaldehyde xylenes (**2**) were not as effective as the flexible bisaldehyde alkanes in shifting the oxygen equilibrium curve.

One bisaldehyde alkene, 1,4-bis(2-carboxy-4-formylphenoxy)-2-*trans*-butene (**2d**), was also synthesized to provide a more rigid linkage between reacting aldehydes than found with the alkane series. The X-ray crystallographic binding was practically identical to that found for the closely related $n = 4$ alkane, **1d**.

(C) (2-Carboxy-4-formylphenoxy)(4-carboxyphenoxy)alkanes (3). The crystal structure of **3d** ($n = 4$)−Hb revealed that it had bound as designed with a similar orientation found for its structural analog in the bisaldehyde series (**1d**, $n = 4$). The acid group that replaced the second aldehyde group did form a salt bridge with Lys 99α as modeled (Figure 2). The region near the covalent Schiff base interaction with Val 1α was well defined while the region near the noncovalent salt bridge with Lys 99α was less well defined (Figure 7). The replacement of one aldehyde with an acid in the class 3 effectors produced the same trend in allosteric properties as found with the bisaldehyde alkanes (Table 1); the strongest allosteric effector activity occurs when the bridging chain is the shortest ($n = 1$ and $n = 2$) and decreases

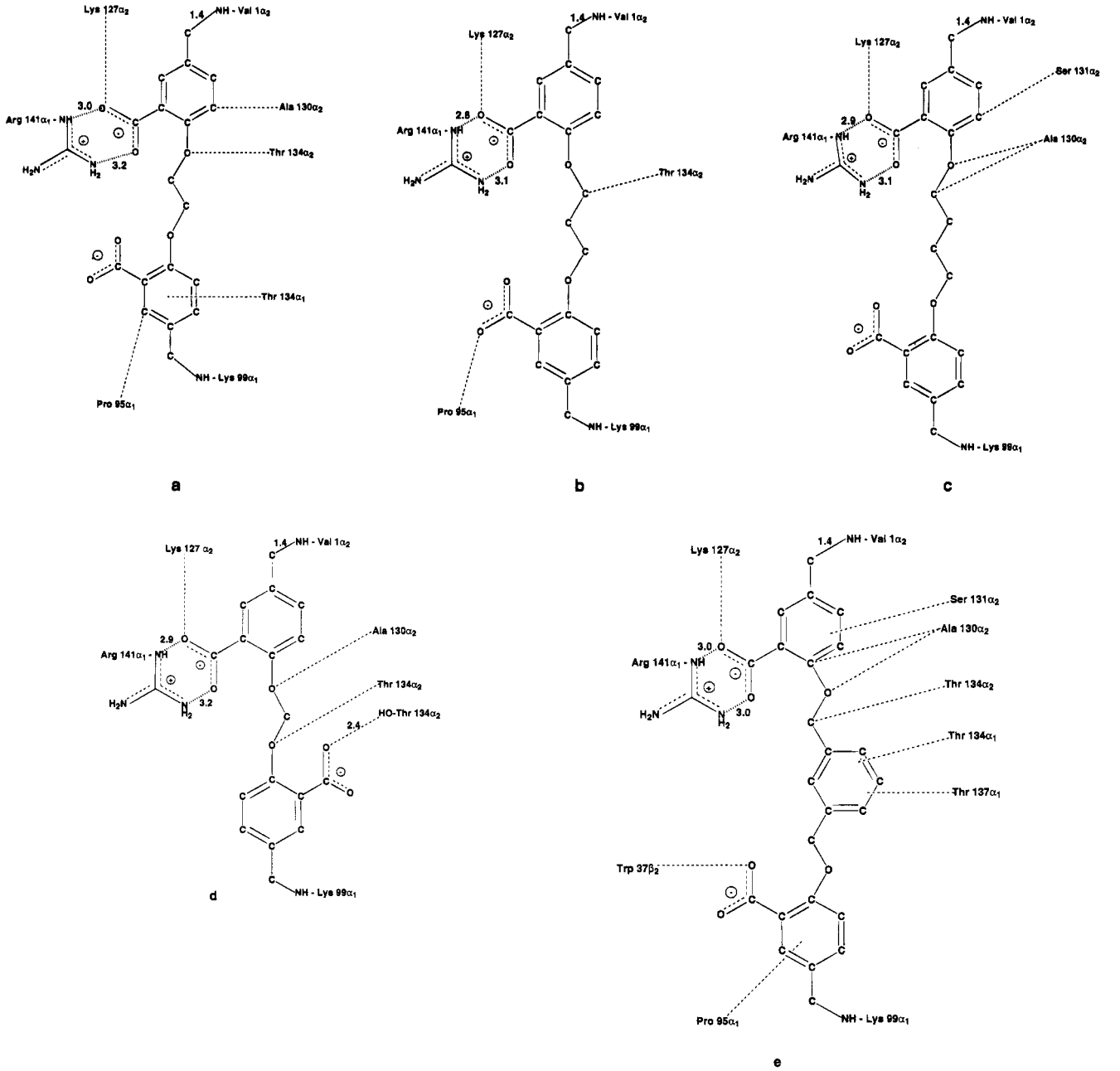

FIGURE 5: This figure shows close contacts with the protein. Dotted lines are to residues that move or are within 4 Å. Specific distances of interest are labeled. Structures: (a) compound **1b**; (b) compound **1c**; (c) compound **1d**; (d) compound **1a**; (e) compound **2a**.

in activity as the chain is lengthened. The general decrease in allosteric effector activity of this class compared to classes 1 and 2 can be attributed to the replacement of a covalent bond by a weaker salt bridge interaction with Lys 99α.

(D) Bis(2-carboxy-4-formylphenoxy) Esters (4). This class was designed to cross-link Val 1α residues and to test the difference in reactivity of the Val 1α N-terminal nitrogen on the effector aldehyde vs ester group. One derivative (**4a**) was chosen for X-ray analysis. The only difference electron density observed was located around the Val 1α N-terminal amino groups, and it overlapped partially with the difference electron density found for 5-FSA (Abraham et al., 1995b). There was no indication of a binding site for the rest of the molecule. If the diester moieties had reacted with Lys residues during T-state crystal growth (discussion below), an amidation product similar to the fumarate bridge that cross-links Lys 99α in deoxy-Hb should have been observed. The diester portion of the molecule, if attached to the effector or Hb, is disordered. The class 4 molecules incubated with Hb in air before reduction of the Schiff base linkage show a small left shift in their oxygen equilibrium curves (Table 1).

Oxygen Equilibrium Measurements on Solutions Obtained from T-State Crystals. Oxygen binding curves were performed on solutions obtained from T-state crystals with the view of obtaining accurate oxygen binding parameters on the purified effector−Hb complexes used in the structural studies. Also, by using the same material for all studies, structure/function correlations would be more consistent.

The Hill plots and corresponding P_{50} values for four bisaldehydes from class 1 (**1a**, **1b**, **1c**, and **1d**) and one monoaldehyde bisacid (**3d**) are presented in Figure 8a. The order of P_{50} shift was parallel to that found for solutions of the same molecules reacted in air before reduction of the

FIGURE 6: Fitting of $n = 1$ (**1a**) to the electron density (molecules in white). Positive contours are in cyan and negative contours are in magenta; the α_1 subunits are in green and the α_2 subunits are in yellow. The single methylene bridge in **1a** is not quite long enough to position an aldehyde group near Lys 99α if symmetry-related molecules are fit. The carboxylate groups on the aromatic ring that covalently binds to Lys 99α of the opposite chain are too close (white and red carboxylates in the center). Positive density around and near Lys 99α indicates that one terminal ring may bind covalently while the other is disordered. The *m*-carboxylate of **1a** forms the same bidentate hydrogen bond and salt bridge with the guanidinium ion of Arg 141α of the opposite subunit (labeled A141 NH2). The other carboxylate may also interact with Thr 134α of the same subunit (close contacts are shown in Figure 5e).

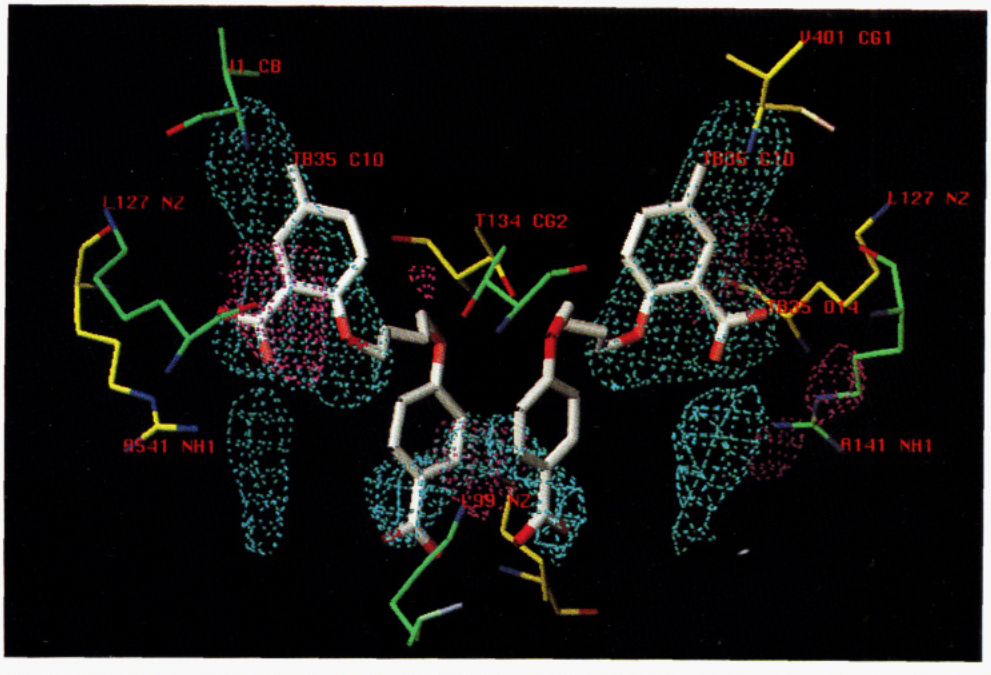

FIGURE 7: This figure shows the fit of compound **3d** ($n = 4$) to the electron density. The positive electron density is in cyan and the negative electron density in magenta; the α_1 subunits are in green and the α_2 subunits in yellow. The density showed that **3d** bound as designed with a similar orientation found for its structural analog in the bisaldehyde series (**1d**, $n = 4$). The acid group that replaced the second aldehyde group is placed in the density near Lys 99α of the opposite subunit (bottom center). The region near the covalent Schiff base interaction with Val 1α was well defined (upper left and right) while the region with the flexible chain (center) did not show density.

Schiff base linkage (Table 1) except that **1b** is shown to be a stronger effector than **1a**. This could be due to differences in degree of reaction of **1b** over **1a** (due to steric repulsion in **1a** as discussed above), if further reaction occurs during T-state crystal growth. These experiments support the conclusion that the strongest acting allosteric effectors are

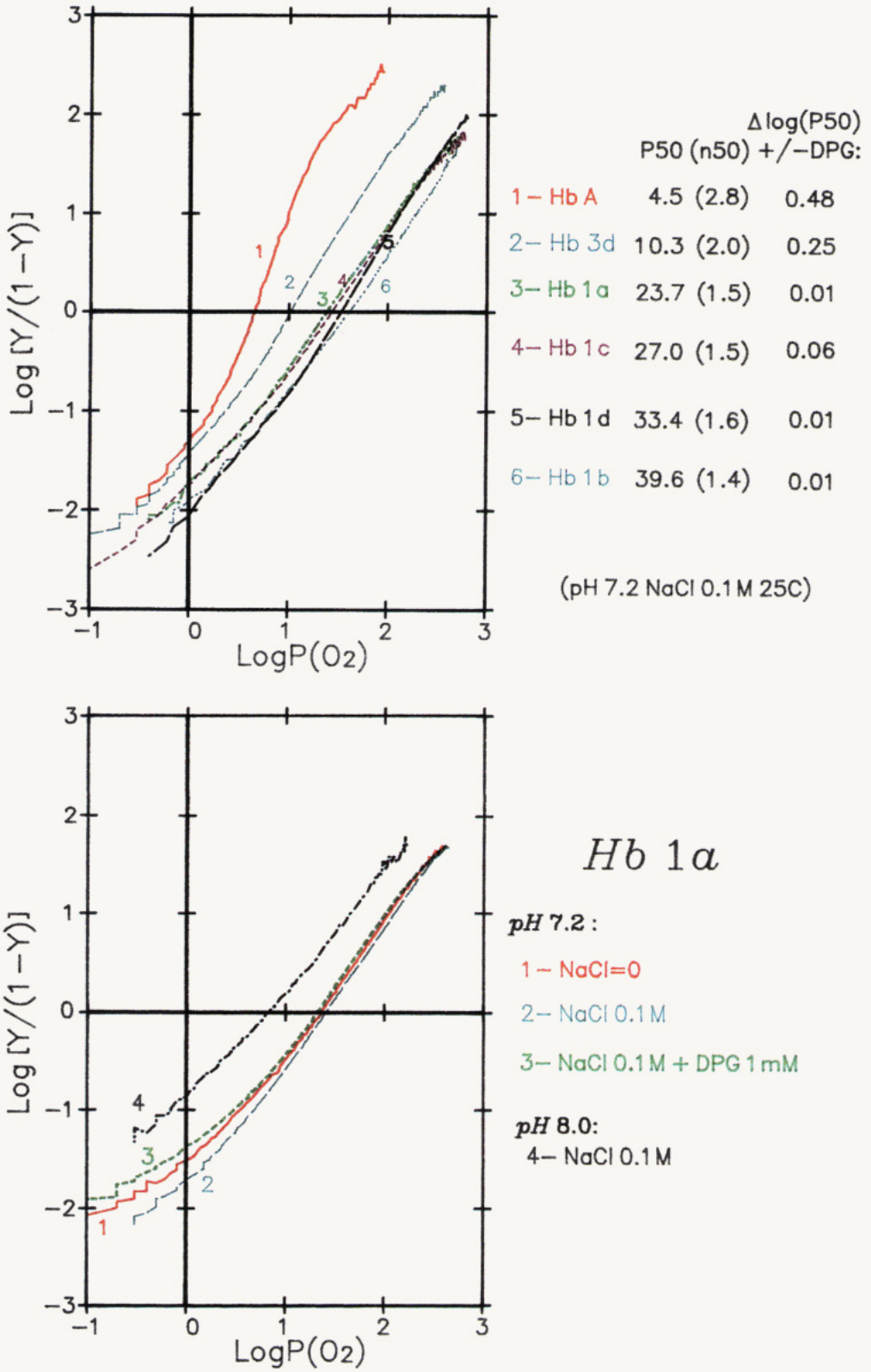

FIGURE 8: (a, top) This figure shows the Hill plots made from solutions taken from the T-state crystals used in the diffraction studies. The P_{50} values are listed to the right with the Hill coefficients (n_{50}). Also shown are the Δ log P_{50} values for ±1 mM DPG. (b, bottom) Hill plots for **1a** (1) without chloride, in 10 mM Hepes buffer, pH 7.2; (2) with 0.1 M NaCl and 50 mM bis-Tris, pH 7.2; (3) with 0.1 M NaCl + 1 mM DPG and 50 mM bis-Tris, pH 7.2; and (4) 0.1 NaCl and 50 mM tris, pH 8.

those with the shortest cross-links between Val 1α and Lys 99α of the opposite subunit. The weakest acting allosteric effector tested was the monoaldehyde **3d**, and this would be expected since it does not covalently link Lys 99α but can only form a salt bridge with the Lys 99α ammonium ion.

Figure 8a shows that the slopes of the Hill plots for the different drug−Hb complexes are all decreased relative to native Hb. This is especially true for compounds **1a**, **1b**, **1c**, and **1d** where the protein has been cross-linked from Val 1α to Lys 99α of the other subunit. The n_{50} values, which

Table 4: Allosteric Parameters for Bisaldehyde Allosteric Effector−HbA Complexes[a]

bisaldehyde effector−HbA complexes	P_{50}, mmHg	n_{50}	L[b]	c[c]	K_R, mmHg	K_T, mmHg	% T_3[d]	i_s[e]	σ[f] × 10^3
HbA	4.5	2.8	$1e^5$	0.0097	0.24	24.7	8	2.5	6
Hb−**1a**	23.7	1.5	$4e^5$	0.0263	1.0	38.0	88	3.6	8
Hb−**1d**	33.4	1.6	$6e^5$	0.0200	1.2	60.0	83	3.0	7
Hb−**3d**	10.3	2.0	$1.5e^5$	0.0200	0.5	25.0	55	3.1	8

[a] Conditions: pH 7.2, 0.1 M NaCl, 0.05 M bis-Tris, 50 μM EDTA, 20 μg/mL catalase, [heme] = 60−70 μM, 25 °C. [b] $L = T_0/R_0$. [c] $c = K_R/K_T$. [d] % $T_3 = (Lc^3)/(1 + Lc^3)$. [e] $i_s = -\log L/\log c$. [f] σ = standard error by point.

are empirical indexes of the cooperativity at 50% oxygen saturation, are close to 1.5. The n_{50} value for **3d** (covalently bound to Val 1α but with only a salt bridge to Lys 99α of the other subunit) is better preserved (2.0). This result supports the idea that the salt bridge between **3d** and Lys 99α does not place as strong a constraint on the T-state as the covalent bond made with Lys 99α by one of the class 1 effectors.

Addition of DPG (1 mM) to native Hb shifts the oxygen binding curve to the right and is expressed by a Δlog P_{50} of 0.48. This value should be compared to those observed for the class 1 modified hemoglobins for which the DPG effect is almost zero (Figure 8a). By contrast, the **3d**−Hb complex differs significantly, with a DPG effect maintained at half the normal value. Preliminary studies with one of the class 1 molecules (**1a**) indicates a normal alkaline Bohr effect and a very low oxygen-linked chloride effect (Figure 8b). The expression of the heterotropic effects exhibited by DPG, chloride anions, and pH (Bohr effect) will be reported separately.

The difference in the DPG effect with class 1 vs 3d may be due to the double cross-linked residues in class 1 or the degree of reaction of the N-terminal nitrogens of the β chains. As mentioned above, there were only small difference densities near the β N-terminal nitrogens of the derivatives studied, indicating the possibility of disordered binding. We conducted sequencing studies to see if the degree of binding to the β N-terminal nitrogens could be determined as well as the overall reaction at both α and β N-termini.

The allosteric constants for three key derivatized hemoglobins (**1a**, **1d**, and **3d**) were determined from the oxygen binding curves using the MWC model (Monod et al., 1965) and are listed in Table 4. The derivatives that lower Hb oxygen affinity the most (**1a** and **1d**) exhibited a significant increase in K_T (binding constant to the T-state) together with a significant increase in the allosteric equilibrium constant (L). As expected, the % T_3 (triligated T-state Hb) and the switchover points (i_s) are much greater than those determined for **3d** (not covalently cross-linked) and the monoaldehyde-derivatized hemoglobins in the accompanying study (Abraham et al., 1995b). Hb cross-linked derivatives **1a** and **1d** exhibit respectively 88%, 83% T_3 and 3.55, 3.34 i_s vs 8% T_3, 2.48 i_s for native control Hb. The allosteric parameters for both **1a** and **1d** indicate a large shift of the allosteric equilibrium toward the T-state. The ΔP_{50} for **1a** is 19.5 and for **1d** 28.9 mmHg. As indicated in the difference maps for the reduced Schiff bases, steric repulsion inhibits two **1a** molecules from simultaneously covalently cross-linking both Lys 99α residues. Therefore the shift in P_{50} for **1a** (one cross-link) would not be expected to be as great as that of **1d** (two cross-links with Lys 99α residues). This difference is also reflected in K_T (Table 4), indicating a much greater constraint is applied by **1d** over **1a**. Interestingly, the % T_3 values do not reflect as great as difference between **1a** and **1d**. This result may indicate that an intrinsic activity difference exists between **1a** and **1d** similar to those observed for noncovalently acting allosteric effectors (Abraham et al., 1995a). We cannot separate out the effect on the oxygen binding curves of binding of **1a** or **1d** to a portion of the β subunit N-terminal Val 1 residues as indicated in Table 3, but the fact that the oxygen binding studies follow the MWC model supports the conclusion that the P_{50} values observed correspond to the major fractions in the electrophoresis which in turn correspond to the agreement between the observed X-ray binding sites and the sequencing results.

The % T_3 and i_s values for **3d**, on the other hand, are lower, as would be expected since only one covalent bond is formed to each Val 1α amino group with only a salt bridge interaction with Lys 99α of the opposite subunit.

The increase in K_T and L (for all three derivatives that lower Hb oxygen affinity) is consistent with the interpretation that they place a greater constraint on the T-state as proposed below, as demonstrated in the accompanying paper (Abraham et al., 1995b), and as found in our other studies with noncovalent acting allosteric effectors (Abraham et al., 1995a).

Sequencing Measurements on Solutions Obtained from T-State Crystals. Sequencing analyses were also carried out on solutions obtained from T-state crystals for six members of class 1 and one member from each of the other three classes to determine the degree of reaction at the N-terminal nitrogens of both chains (Table 3). The normal Edman degradation reaction utilizes phenyl isothiocyanate that reacts with a primary amine (N-terminal group of peptides) and forms a cyclic PTH derivative. The PTH-amino acid is then characterized by retention times and measured in picomoles. If the aldehyde effectors do not react with any N-terminal valines (on either chain), the ratio of the concentrations of [Val-PTH]/[each PTH derivative from residues **2**−**5**] would be 2/1 since there are no other identical residues on both chains at residues **2**−**5**. If the N-terminal amino groups do react, we assumed that the reacted and reduced aldehydes (secondary amines) would prevent sequencing of the entire chain in the same manner that an acylated N-terminal amino acid does. Therefore, we expected to only see sequencing of the unreacted α and β chains. The amount of Val-PTH derivative was markedly reduced as expected. Unexpectedly, both the α and β chains sequenced normally. This means that an aldehyde-Val 1-PTH derivative is produced by reaction of phenyl isothiocyanate with the secondary amine of the reduced aldehyde−Hb complex, permitting the next residues to sequence normally. This idea was tested and confirmed as described in the accompanying paper (Abraham et al., 1995b).

Table 3 shows that three to three plus chains of the tetramer were reacted with the aldehyde effectors at the Val 1α and/or Val 1β N-terminal amino groups. The sequencing results are consistent with complete reaction of both N-terminal amino groups of the α chains, in agreement with the crystallographic studies that show symmetry-related pairs of effectors bound to Val 1α. If the quantitative comparison of PTH peaks reflects the sequencing as described above, 50% or more of the β chains appear to be reacted with the

aldehydes in T-state crystals. Therefore, the small peaks (the size of one or two atoms at most) near the β N-terminal amino groups must represent the presence of disordered aldehyde molecules attached to a portion of the Val 1β residues. These disordered attached effectors would not be visible in the difference map due to their rotation in space with little or no preferred conformation. The sequencing experiments are in keeping with the oxygen equilibrium measurements that show little DPG effect for **1a**, **1b**, **1c**, and **1d** while 50% is observed for **3d**. The sequencing indicates a 2-fold higher reaction of **1a**, **1b**, **1c**, and **1d** at the terminal nitrogens compared with **3d** (Table 3).

Characterization of the Number of Binding Sites. A major goal in this study was to locate the primary and secondary binding sites for a large number of allosteric effectors and cross-linking agents. The crystal structural analysis provided a composite picture of these sites and their relative occupancies to each other. In general, the crystal lattice will not permit significant amounts of nonspecific binding (especially on the surface) without distortion of the crystal and loss of isomorphous properties. We have previously observed crystal lattice distortion and loss of isomorphous properties by increasing the amount of allosteric effector to observe the limit of the number of binding sites (Abraham et al., 1983). It has been our experience that difference electron density maps are very sensitive in determining the number of ordered binding sites.

The number of binding sites observed in the X-ray maps and those indicated by sequencing (i.e., reaction at the β1 Val residues) were further characterized by comparison with the number of bands observed by electrophoresis. Isoelectric focusing electrophoresis was run (4 °C) on solutions made from dissolved crystals that had been reacted with effectors **1a**, **1b**, **1c**, **1d**, and **3d** for diffraction studies. The major bands in the isoelectric focusing electrophoresis (usually two) can be related to the number of sites observed in the X-ray difference maps and the total number of Val 1α and β residues indicated in the sequence analysis. Any small satellite bands were attributed to low occupancies not detectable in the diffraction study ($<10-15\%$).

With effectors from class 1, where cross-linking Lys 99α and reaction at both α and β N-termini can occur in varied degrees, a variety of electrophoresis peaks were expected. The following four major peaks would be expected with these derivatives: Val 1α-unreacted-Val 1β-unreacted-Lys 99α-unreacted (unreacted Hb); Val 1α-reacted-Val 1β-unreacted-Lys 99α-unreacted; Val 1α-reacted-Val 1β-reacted-Lys 99α-unreacted; and Val 1α-reacted-Val 1β-reacted-Lys 99α-reacted. The electrophoresis patterns, in general, exhibited two to three major peaks, in agreement with difference maps that show the strongest electron density peaks at Val 1α cross-linked in varying degrees with Lys 99α and the sequencing experiments that show about three of the four Val residues are modified. Therefore, the two to three primary bands reflect the variety of reaction possibilities outlined above. The covalent cross-linking derivatives from class 1 do not show the presence of unreacted Hb and only the monoaldehyde bisacid **3d** exhibited a band for unreacted Hb.

Specifically, effector−Hb complex **1a** showed two major bands with a smaller band and no unreacted Hb band (reaction at both α Val 1 residues, the β Val 1 residues, and some of the Lys 99 residues as shown above), **1b** showed two major bands and two secondary bands with two small satellites (this indicates the same primary reaction sites as **1a** with the distribution of peaks showing more reaction at Lys 99α, i.e., less charge), **1c** showed one primary band with three small satellites, and **1d** showed two major bands with three small satellites. The monoaldehyde bisacid **3d** showed a simpler pattern with two major bands and two weak satellites (also in agreement with what would be expected by primary reaction at Val 1α, some reaction at Val 1β (as indicated in the sequencing), and in this case some unreacted Hb. From the characterization of the crystals presented here, along with those in the accompanying paper (Abraham et al., 1995b), it appears clear that the X-ray difference maps give a very good first-order indication of the primary binding sites and that these sites are related to the observed oxygen binding properties as discussed here.

DISCUSSION

Can the Same Aldehyde Allosteric Effector Bind to the Same Protein Residue in Both Allosteric States? X-ray analyses prepared from crystals incubated and reduced under both oxy and deoxy conditions for two of the bisaldehyde alkanes (**1a**, $n = 1$, and **1c**, $n = 3$) showed exactly the same binding mode in the T-state electron density maps. Although the degree of reaction under R- and T-state conditions may be different, the aldehydes must bind to Val 1α in both states since incubation and reduction under R- or T-state conditions produces identical crystal structures. A new binding orientation cannot occur after reduction of the Schiff base since a nonhydrolyzable cross-link freezes the points of attachment to the protein. This result combined with oxygen equilibrium studies and sequencing experiments described above show that (1) Val 1α binds the aldehydes in both T- and R-states, (2) during T-state crystallization, and in the presence of excess aldehyde and reducing agent, further reaction may occur at the β N-terminal amino groups, (3) symmetry-related pairs of effectors cross-link Val 1α and Lys 99α, and (4) once the complete covalent cross-linked reaction has been obtained in the T-state, the protein must provide sufficient room for the symmetry-related cross-linked pair of molecules to exist in the R-state during reoxygenation.[3]

What Structural Features of the Aldehyde Effectors Can Be Modified To Increase the Constraint in the T-State and Produce a Desired Degree of Shift in the Allosteric Equilibrium? In the accompanying paper (Abraham et al., 1995b), it was shown that monoaldehyde effectors that add additional constraint to the T-state produce low-affinity hemoglobins that *right shift* the oxygen equilibrium curve. The added constraint is due to an intersubunit salt bridge between the effector (covalently bound to Val 1α) and the guanidinium ion of Arg 141α of the opposite subunit. The much stronger acting allosteric effectors studied here (class 1) not only maintain this same inter-α-subunit carboxylate salt bridge with the Arg 141α guanidinium ion but also

[3] The difference between the R- and T-state cavity at the top of the α subunits does not differ significantly (14.3 Å in the R-structure and 16.2 Å in the T-structure between Val 1α terminal nitrogens). However, the cavity narrows in the R-state as it proceeds toward the Lys 99α residues, and Arg 141α and Thr 134α, which are very close in the R-state structure, must move to accommodate the covalently attached hemoglobin effector complex during oxygenation. Therefore, a greater degree of reaction with Hb would be expected to occur in T-state Hb when the effectors are oriented diagonally down the central water cavity.

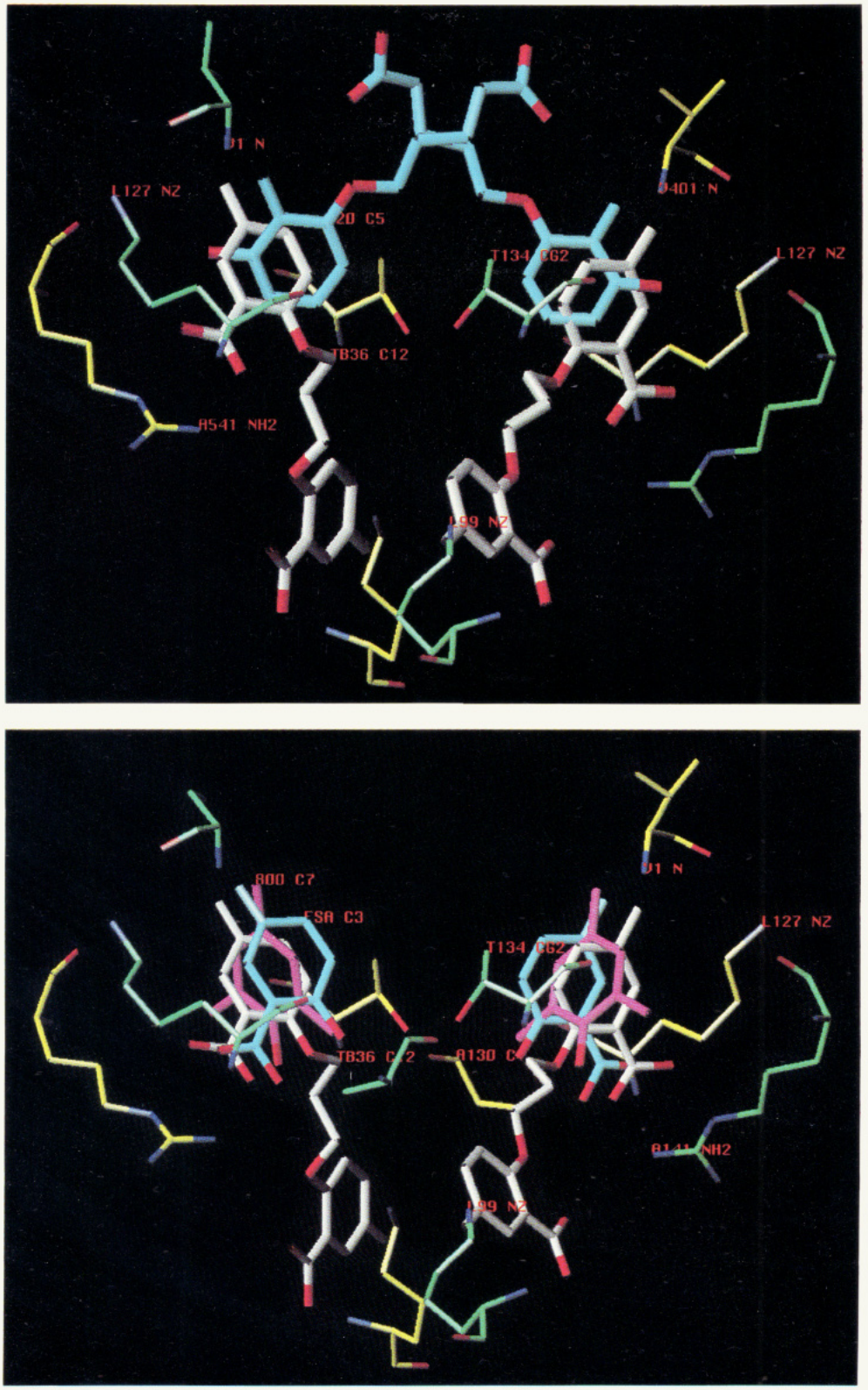

FIGURE 9: (a, top) This figure shows the superimposed binding modes of **1c** (white) and 12C79 (blue). The α_1 subunits are in green and the α_2 subunits are in yellow. Both effectors are bound to Val 1α N-terminal amino groups. Note that the *para* position of **1c** points diagonally downward toward Lys 99α of the opposite subunit. The *m*-carboxylate forms a salt bridge interaction with Arg 141α, labeled A141 NH1, of the opposite subunit (middle left and right). 12C79 points its acid chain diagonally upward (toward the center) and does not form any contacts with any residues on the opposite α chains. (b, bottom) This figure shows the superimposed binding sites for 5-FSA (blue), DMHB (purple), and **1c** (white). The binding of **1c** is the same as described in (a). The lack of a carboxylate on DMHB permits the aromatic ring to turn with no close contacts with the opposite subunit. The 5-FSA binding site is mimicked by the class 1 effectors so that their reactive chains attached in the *para* position to the phenolic hydroxyl are oriented from the start toward Lys 99α.

provide additional constraint via a second covalent bond that cross-links the α subunits from Val 1α of one subunit with Lys 99α of the opposite subunit. It appears that the degree of additional constraint placed on the T-state by the cross-link with Lys 99α varies with the flexibility of the chain length. The shorter bridging chains produce the largest shifts

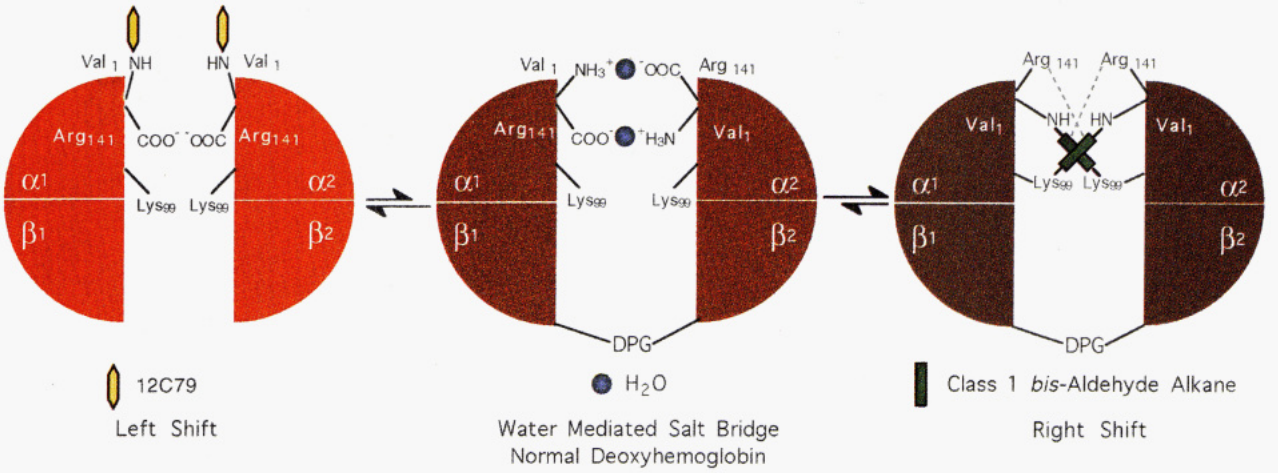

FIGURE 10: This figure summarizes the proposed hypothesis to explain the opposite allosteric effects demonstrated by similar aldehyde acids that bind to Val 1α (for example, see Figure 9a). Fermi (1975) has proposed that it appears likely that the amino and carboxyl termini of the opposite α chains of deoxyhemoglobin are involved in some form of linkage, perhaps mediated by a water molecule, that is broken upon oxygenation to the R-state. The termini and water bridge interaction is shown in the central diagram and depicts its contribution to the normal constraint of the T-state. Also possible is the stabilization of T-state Hb (center) by an anion binding site linking the N-terminal amino group of Val 1α with the guanidinium ion of Arg 141α of the opposite subunit (O'Donnell et al., 1979; Nigen et al., 1980). When DPG, the natural allosteric effector, is bound to the bottom of the central water cavity tying together the β subunits, further constraint is applied to the T-state and the oxygen equilibrium is shifted to the right. When the allosteric effectors from class 1 are reacted with Hb, they also add further constraint to the T-state by forming interchain cross-links between Val 1α and Lys 99α residues and intersubunit salt bridges between Val 1α and Arg 141α. This combination of bonds and interactions provides a strong shift of the oxygen equilibrium to the right and produces a hemoglobin with very low affinity for oxygen. On the other hand, effectors that left shift the oxygen equilibrium curve to produce high-affinity hemoglobins bind to Val 1α with no intersubunit T-state interactions, narrow the central water cavity inhibiting nonspecific chloride binding (Perutz et al., 1993), and disrupt the T-state salt, anion binding, and/or proposed water-mediated bridge between the opposing termini of the α chains. This is depicted in the left-hand diagram with the allosteric effector 12C79. Figure 9 provides structural details that provide the basis for this figure.

in the allosteric equilibrium. Therefore, the tighter the cross-link, the greater the constraint on the T-state and the stronger the allosteric effect. In a sense, the new bisaldehyde effectors of class 1 might be termed "*molecular ratchets*"; they can be tightened or loosened to obtain the desired shift in the allosteric equilibrium. The new effectors might also be useful as tools to explore allosteric phenomena in other systems.

What Key Structural Components of the Aldehyde Effectors Are Necessary To Orient Their Reactive Chains To Cross-Link or Interact with Desired Protein Residues? The effectors **1a** and **1b** are ideally spaced to cross-link the two terminal Val 1α nitrogens *or* Val 1α with Lys 99α of the opposite subunit (Figure 1b). Thus far, no bis- (or mono-) aldehydes that we have studied bind in a horizontal position spanning the top of the α subunits between the Val 1α amino groups as proposed for 12C79 (Beddell et al., 1976). The bound aldehydes all point vertically or diagonally along the cavity wall.

The driving force for this orientation appears to be the position of a key functional group. Every aldehyde effector studied in this work and the accompanying paper, which contains a *m*- or *p*-carboxyl group on the aromatic ring covalently bound to Val 1α, points that ring diagonally down the central water cavity toward Lys 99α. This orientation must be influenced by the intersubunit salt bridge between the effector carboxyl group and the guanidinium ion of Arg 141α as illustrated for **1c** (Figure 9a). Removal of the carboxylate in 5-FSA with a shift of the *o*-hydroxyl to the *para* position, as found in 3,5-dimethyl-4-hydroxybenzaldehyde (DMHB) (Abraham et al., 1995b), frees this ring to rotate without any interaction with the guanidinium ion of Arg 141α (Figure 9a). DMHB makes no contact with the opposite α subunit and left shifts the oxygen equilibrium curve. On the other hand, the presence of a functional group such as a phenolic hydroxyl at the *ortho* position, as positioned in 12C79, shifts the aromatic ring diagonally up the central water cavity. The *o*-hydroxy group forms a hydrogen bond with the N-terminal nitrogen to stabilize this conformation (Figure 9b).

The longer more flexible chain derivatives that could have overcome the direction set by the *m*-carboxylate−guanidinium salt bridge with Arg 141α by folding back in a U-shape to cross-link the two Val 1α N-terminal nitrogens did not. It appears that, in general, *long flexible molecules prefer to bind along cavity walls, like double-sided molecular sticky tape*, rather than span large open spaces with few chances for interaction. New investigations are underway to determine if well-positioned functional groups can orient a reactive chain to cross-link the N-terminal nitrogens of Val 1α.

What Structural Features of the Aldehyde Effectors Are Responsible for the Observed Direction in Shift of the Allosteric Equilibrium? It is easy to understand how allosteric effectors can regulate the allosteric equilibrium in either direction by binding to and stabilizing either the R- or T-state structure. However, at first appearance, it is more difficult to understand how different allosteric effectors can bind to the same protein residue reacted in the same allosteric state yet exhibit opposite regulatory properties. For example, 12C79 and the class 1 effectors (both are aromatic aldehyde acids) when incubated under R-state conditions bind to Val 1α and produce opposite allosteric effects. 12C79 and analogs powerfully left shift (Beddell et al., 1984) while the bisaldehyde alkanes from class 1 powerfully right shift the oxygen equilibrium curve.

The results in this paper add confirmation to the hypothesis presented in the accompanying paper (Abraham et al.,

1995b). Adding additional constraint to the T-state by cross-linking Val 1α with Lys 99α of the opposite subunit does shift the allosteric equilibrium further to the right as proposed (Figure 10). It appears that any effectors bound in the central water cavity, whether they left or right shift the oxygen equilibrium curve, will inhibit the oxygen-linked chloride effect as demonstrated with compound **1a** (Figure 8b). As reported (Abraham et al., 1995b), the reduced chloride effect is probably due to both the addition of negative charges in the central water cavity by the effector acid groups and the narrowing of the central water cavity caused by effector binding. These results also confirm our earlier studies that indicate that Lys 99α is a key residue for interaction to produce low-affinity hemoglobins (Wireko & Abraham, 1991; Abraham et al., 1992b).

New effector molecules are needed to further test the hypothesis for producing low-affinity hemoglobins. The hypothesis states that effectors that left shift the oxygen equilibrium curve to produce high-affinity hemoglobins bind to Val 1α with no intersubunit T-state interactions, narrow the central water cavity inhibiting nonspecific chloride binding (Perutz et al., 1993), and disrupt the T-state salt or proposed water-mediated or anion bridge between the opposing termini of the α chains (Fermi, 1975; O'Donnell et al., 1979; Nigen et al., 1980). New molecules with substitutions on one of the bis(*o*-hydroxyl) groups in the 12C79 framework will be modeled to bind vertically along the cavity wall without intersubunit contacts. These will be oriented toward the surface and will have chains that extend out of the central water cavity. Such molecules would be of interest as potential antigelling and antisickling agents. They should act directly by inhibiting sickle Hb polymer formation at the contact region of the central water cavity in the sickle polymer and indirectly by shifting the allosteric equilibrium toward the more soluble R-state.

Correlations have previously been found between log P_{50} and bridging distances for hemoglobins cross-linked between Val $1\beta_1$ and Lys 82 β_2 as well as between Lys 82 of each β subunit (Jones et al., 1993). Studies such as those presented here and in the Jones et al. (1993) paper may make it possible in the future to "taylor-make" cross-linking agents with the desired allosteric properties to act as blood substitutes as well as increase our understanding of allosteric phenomena.

ACKNOWLEDGMENT

This paper is dedicated to the 80th birthday celebration for Dr. Max F. Perutz held in London on Sept 23, 1994. The authors gratefully acknowledge helpful discussions with Drs. Max Perutz, Gajanan Joshi, Eugene Orringer, and Gary Ackers and technical assistance by Mr. Mark Eaton (Richmond), Jayashree Panikker (Richmond), Frank A. Fornari (Richmond), and Mrs. G. Caron (Paris).

REFERENCES

Abraham, D. J., Perutz, M. F., & Phillips, S. E. V. (1983) *Proc. Natl. Acad. Sci. U.S.A. 80*, 324.
Abraham, D. J., Peascoe, R. A., Randad, R. S., & Panikker, J. (1992a) *J. Mol. Biol. 227*, 480.
Abraham, D. J., Wireko, F. C., Randad, R. S., Poyart, C., Kister, J., Bohn, B., Liard, J.-F., & Kunert, M. P. (1992b) *Biochemistry 31*, 9141.
Abraham, D. J., Kister, J., Joshi, G. S., Marden, M. C., & Poyart, C. (1995a) *J. Mol. Biol. 248*, 845.
Abraham, D. J., Safo, M. K., Boyiri, T., Danso-Danquah, R. E., Kister, J., & Poyart, C. (1995b) *Biochemistry 34*, 15006−15020.
Arnone, A. (1972) *Nature 237*, 146.
Beddell, C. R., Goodford, P. J., Norrington, F. E., Wilkinson, S., & Wootton, R. (1976) *Br. J. Pharmacol. 57*, 201.
Beddell, C. R., Goodford, P. J., Kneen, G., White, R. D., Wilkinson, S., & Wootton, R. (1984) *Br. J. Pharmacol. 82*, 397.
Chatterjee, R., Walder, R. Y., Arnone, A., & Walder, J. A. (1982) *Biochemistry 21*, 5901.
Evans, P. (1985) *Med. Res. Counc. Lab. Mol. Biol.*, Cambridge, U.K.
Fermi, G. (1975) *J. Mol. Biol. 97*, 237.
Fermi, G., Perutz, M. F., Shaanan, B., & Fourme, R. (1984) *J. Mol. Biol. 175*, 159.
Jones, R. T., Head, C. G., Fujita, T. S., Shih, D. T.-B., Wodzinska, J., & Kluger, R. (1993) *Biochemistry 32*, 215.
Kister, J., Poyart, C., & Edelstein, S. J. (1987) *J. Biol. Chem. 262*, 12085.
Kluger, R., Jones, R. T., & Shih, D. T.-B. (1994) *Artif. Cells, Blood Substitutes, Immobilization Biotechnol. 22*, 415.
Lalezari, I., Rahbar, S., Lalezari, P., Fermi, G., & Perutz, M. F. (1988) *Proc. Natl. Acad. Sci. U.S.A. 85*, 6117.
Manning, L. R., & Manning, J. M. (1988) *Biochemistry 27*, 6640.
Monod, J., Wyman, J., & Changeux, J. (1965) *J. Mol. Biol. 12*, 88.
Nigen, A. M., Manning, J. M., & Alben, J. O. (1980) *J. Biol. Chem. 255*, 5525.
O'Donnell, S. O., Mandaro, R., Schuster, T. M., & Arnone, A. (1979) *J. Biol. Chem. 254*, 12204.
Perutz, M. F. (1968) *J. Cryst. Growth 2*, 54.
Perutz, M. F., Fermi, G., Poyart, C., Pagnier, J., & Kister, J. (1993) *J. Mol. Biol. 233*, 536.
Randad, R. S., Mahran, M. A., Mehanna, A. S., & Abraham, D. J. (1991) *J. Med. Chem. 34*, 752.
Still, W. C., Mohamadi, F., Richards, N. G. J., Guida, W. C., Lipton, M., Liskamp, R., Chang, G., Hendrickson, T., Degunst, F., & Hasel, W. (1989) in *MACROMODEL*, Department of Chemistry, Columbia University, New York.
Wireko, F. C., & Abraham, D. J. (1991) *Proc. Natl. Acad. Sci. U.S.A. 88*, 2209.
Wireko, F. C., Kellogg, G. E., & Abraham, D. J. (1991) *J. Med. Chem. 34*, 758.

BI950435C